═══REVIEW COMMONS MANUSCRIPT═══

IMPORTANT:

- Manuscripts submitted to Review Commons are peer reviewed in a journal-agnostic way.
- Upon transfer of the peer reviewed preprint to a journal, the referee reports will be available in full to the handling editor.
- The identity of the referees will NOT be communicated to the authors unless the reviewers choose to sign their report.
- The identity of the referee will be confidentially disclosed to any affiliate journals to which the manuscript is transferred.

GUIDELINES:

- For reviewers: https://www.reviewcommons.org/reviewers
- For authors: https://www.reviewcommons.org/authors

CONTACT:

The Review Commons office can be contacted directly at: office@reviewcommons.org

Med12 cooperates with multiple differentiation signals to enhance embryonic stem cell plasticity

Max Fernkorn[1], Christian Schröter[1,*]

[1]Department of Systemic Cell Biology, Max Planck Institute of Molecular Physiology, 44227 Dortmund, Germany

*Correspondence: christian.schroeter@mpi-dortmund.mpg.de

Abstract

Cell differentiation results from coordinated changes in gene transcription in response to combinations of signals. FGF, Wnt, and mTOR signals regulate the differentiation of pluripotent mammalian cells towards embryonic and extraembryonic lineages, but how these signals cooperate with general transcriptional regulators is not fully resolved. Here, we report a genome-wide CRISPR screen that reveals both signaling components and general transcriptional regulators for differentiation-associated gene expression in mESCs. Focusing on the Mediator subunit *Med12* as one of the strongest hits in the screen, we show that it regulates gene expression in parallel to FGF and mTOR signals. Loss of *Med12* is compatible with differentiation along both the embryonic epiblast and the extraembryonic primitive endoderm lineage, but pluripotency transitions are slowed down, and the transcriptional separation between epiblast and primitive endoderm identities is enhanced in *Med12*-mutant cells. These cellular phenotypes correlate with reduced biological noise upon loss of *Med12*. These findings suggest that *Med12* regulates cellular plasticity through the priming of transcriptional changes during differentiation, thereby modulating the effects of a broad range of signals.

Introduction

Cell differentiation during development manifests in expression changes of large gene modules that are triggered by extracellular signals and sequence-specific transcription factors. In response to such stimuli, cells must both be able to faithfully mount complex transcriptional responses, as well as maintain plasticity to be able to adapt to changing environments. Knowledge of the molecular regulators that balance faithful differentiation responses and plasticity is therefore of key importance for a mechanistic understanding of cell differentiation. The earliest cell differentiation events of mammalian embryogenesis first segregate the extraembryonic trophoblast from the inner cell mass (ICM). In a second step, the ICM further differentiates into extraembryonic primitive endoderm (PrE) and the pluripotent embryonic epiblast (Epi), which ultimately forms the fetus (Chazaud & Yamanaka, 2016). Subsequently, epiblast cells transition from the naïve pluripotent state at pre-implantation to formative and then primed pluripotency as they prepare for germ layer differentiation (Kalkan & Smith, 2014; Nichols & Smith, 2009; Smith, 2017). Embryonic stem cells (ESCs) allow modeling both the differentiation towards an extraembryonic PrE identity, as well as transitions between different pluripotent states. Mouse ESCs (mESCs) can either be maintained in medium containing serum and the cytokine LIF, or in a ground state of pluripotency using serum-free N2B27 medium supplemented with LIF and two small molecule inhibitors that activate Wnt/beta-Catenin signaling and inhibit FGF/ERK signaling, respectively (2i + LIF; Ying et al., 2008). Efficient PrE differentiation from mESCs can be achieved from ground state pluripotency by the forced expression of GATA transcription factors together with active FGF/ERK signaling (Fujikura et al., 2002; Schröter et al., 2015; Wamaitha et al., 2015). Transitions between pluripotency states in contrast can be triggered by the removal of small molecule inhibitors from the culture medium alone (Kalkan et al., 2017; Neagu et al., 2020). Together with experiments in the mouse embryo, these stem cell models have provided a comprehensive picture of the signaling control of the early lineage transitions in the mammalian embryo. Both PrE differentiation and exit of epiblast cells from naïve towards formative and primed pluripotency require FGF/ERK signaling as well as Wnt signaling inhibition (Athanasouli et al., 2023; Chazaud & Yamanaka, 2016; Kang et al., 2013; Nichols et al., 2009). PrE differentiation further benefits from LIF signaling (Morgani & Brickman, 2015), whereas the progression of epiblast cells is promoted by the Notch signaling effector RBPJ (Kalkan et al., 2019), and the mTOR signaling effector TFE3 (Betschinger et al., 2013; Villegas et al., 2019).

Developmental signaling systems often culminate in the activation or deactivation of sequence-specific transcription factors. In eukaryotes, transmission of such transcription factor activity changes into altered RNA polymerase activity at specific promoters requires

61 large multiprotein assemblies such as the Mediator complex that physically bridges between
62 transcription factors and the basal transcriptional machinery (Soutourina, 2018). The
63 mammalian Mediator complex is formed by up to 30 subunits. It can be subdivided into a head,
64 a core and a tail domain, and the transiently associated CDK8 module which consists of four
65 subunits: the CDK8 kinase, CCNC, MED12, and MED13 (Luyties & Taatjes, 2022; Soutourina,
66 2018). Unperturbed Mediator function is required for expression of most protein-coding genes
67 (Soutourina, 2018). Still, individual Mediator subunits have been linked to transcriptional
68 changes in response to specific signaling systems. Deletion of *Sur2,* which encodes the
69 MED23 subunit, for example abrogates transcriptional activation downstream of ERK-MAPK
70 signaling in mESCs (Stevens et al., 2002). The CDK8 module in particular has been implicated
71 in directing rapid changes in gene expression patterns in response to various stimuli, such as
72 serum stimulation (Donner et al., 2010; Luyties & Taatjes, 2022). Furthermore, CDK8 inhibition
73 in mouse and human ESCs impairs pluripotency exit, mirroring effects of MEK/ERK inhibition
74 (Lynch et al., 2020). MED12, which activates CDK8 function in the kinase module (Knuesel et
75 al., 2009; Park et al., 2018), is essential for axis elongation and the activation of Wnt target
76 genes during mouse development (Rocha et al., 2010). Together, these works suggest that
77 the transmission of specific developmental signals to RNA polymerase II activity can be
78 mapped to specific Mediator subunits. How general these mappings are or whether they are
79 context-dependent is however not clear. It is also not known how interference with Mediator
80 activity in pluripotent cells affects the balance between faithful differentiation lineage plasticity.
81 Here, we aim at identifying factors that mediate transcriptional changes in response to
82 signaling events during early mammalian cell differentiation, using the expression of a
83 *Spry4*$^{H2B\text{-}Venus}$ reporter allele as read-out in a genome-wide CRISPR screen. This reporter is
84 an established indicator of developmental FGF/ERK signals, and its expression is switched
85 on in both Epi and PrE cells during preimplantation development (Morgani et al., 2018). Our
86 screen returns both known and new signaling inputs into *Spry4*$^{H2B\text{-}Venus}$ reporter expression,
87 as well as several components of the Mediator and Elongator complexes. Using epistasis
88 analysis, we demonstrate that *Med12*, one of the strongest hits in the screen, functions
89 independently of and in parallel to the FGF and mTOR signaling systems in pluripotent cells.
90 Functional assays showed that, while not strictly required for lineage transitions, loss of *Med12*
91 leads to impaired signal responsiveness during pluripotency transitions, as well as reduced
92 mRNA levels and noise during extraembryonic cell differentiation. Collectively, these results
93 point to new signal-independent functions of *Med12* that promote cellular plasticity during
94 lineage transitions in early development.

Results

A genome-wide CRISPR screen identifies signaling and transcriptional regulators of *Spry4* expression

The differentiation of pluripotent cells towards different lineages rests on transcriptional changes triggered by extracellular signals. To identify effectors of signal-regulated gene expression during cellular differentiation, we performed a genome-wide CRISPR screen using the expression of a Sprouty4 reporter as a read-out (Hanna & Doench, 2020; Morgani et al., 2018; Fig. 1A). We chose Sprouty4 because it is a known target gene of developmental FGF signals, and shows strong expression changes upon both Epi and PrE differentiation (Morgani et al., 2018; Fig. 1 Supp 1). In serum + LIF medium, the *Spry4* reporter is expressed due to paracrine FGF signals. We generated Cas9-expressing *Spry4*:H2B-Venus reporter cells and transduced them with the Brie gRNA library targeting protein-coding genes (Doench et al., 2016). To identify positive and negative regulators of *Spry4* reporter expression, we flow sorted cells with decreased and increased fluorescence at 6 and 9 days after transduction, and determined enriched guides in sorted fractions (Fig. 1A). We first analyzed perturbations leading to reduced reporter expression. Gene-targeting gRNAs were more strongly enriched in the sorted fractions compared to non-targeting controls (Fig. 1B, Fig. 1 Supp 2, Supp Table 1). We used the robust rank algorithm (RRA; W. Li et al., 2014) to combine information from multiple gRNAs and to rank genes in each of the four conditions (1% and 5% gate at both day 6 and day 9, Supp Table 1). This analysis revealed up to 17 individual genes with an FDR ≤ 0.05, and up to 26 genes with an FDR ≤ 0.2 (Fig. 1C, Fig. 1 Supp 2). We compiled a list of hits by selecting genes that were detected with an FDR of ≤ 0.05 in one condition, or with an FDR of ≤ 0.2 in at least two conditions (Fig. 1D). Protein-protein interaction network analysis with String-DB revealed that most of our hits fell into a small number of groups that were highly connected and associated with specific molecular functions (Szklarczyk et al., 2015; Fig. 1E). One of these groups contained the FGF signaling genes *Fgfr1, Grb2, Sos1,* and *Ptpn11*, as would be expected given the strong regulation of *Spry4* by FGF signaling. Another group contained several genes involved in protein glycosylation and specifically the synthesis of heparan sulfates, such as *Slc35b2*, *Ext1*, *Ext2*, and *Extl3*. Heparan sulfates are crucial co-factors for efficient FGF signaling (Ornitz & Itoh, 2015). Since pooled CRISPR screens detect mainly cell-autonomous functions of gene perturbations, the appearance of these hits indicates that surface-tethered heparan sulfates determine a cell's responsiveness to FGF signaling. Three further groups contained genes associated with ribosome biogenesis and translation (*Rpl9*, *Rpl18*, *Eif3i* and *Dhx37)*, as well as genes of the Elongator (*Elp2 – 6*, *Ikbkap*

129 and *Kti12*) and Mediator complexes (*Med10, Med12, Med16, Med24* and *Med25*, Fig. 1E),
130 raising the possibility that these factors could have gene- or signal-specific functions in
131 mESCs.
132 Next, to validate selected hits in an independent experimental setting, and to evaluate their
133 effect size, we knocked out individual candidate genes using the most enriched gRNA from
134 the screen. Since we were interested in mechanisms of transcriptional regulation, we focused
135 on hits related to the Mediator and Elongator complexes, but also included *Grb2* and *Ptpn11*
136 as a reference to evaluate the effects of perturbing FGF signal transduction, and *Sox2* and
137 *Fam98b* as candidates that could not clearly be linked to a functional group (Fig. 1E). Flow
138 cytometry showed that knockout of all tested candidates led to a reduction of mean
139 *Spry4*:H2B-Venus fluorescence levels, albeit to a different degree: Knockout of components
140 of the Elongator complex as well as *Fam98b* and *Sox2* affected Sprouty4:H2B-Venus
141 expression only mildly, whereas knockout of the FGF signaling genes *Grb2* and *Ptpn11* had
142 the strongest effect, although they did not reach the reduction achieved via pharmacological
143 inhibition of FGF signal transduction with the MEK inhibitor PD0325901 (PD03) (Fig. 1F, G).
144 Knockout of Mediator components reduced *Spry4*:H2B-Venus levels to different degrees, with
145 *Med12* having the strongest effect, reducing *Spry4*:H2B-Venus levels to 35.3% ± 1.6%
146 compared to control (Fig. 1F, G). Thus, our screen and validation establish *Med12* as a strong
147 candidate regulator of signal-dependent gene expression in mESCs.

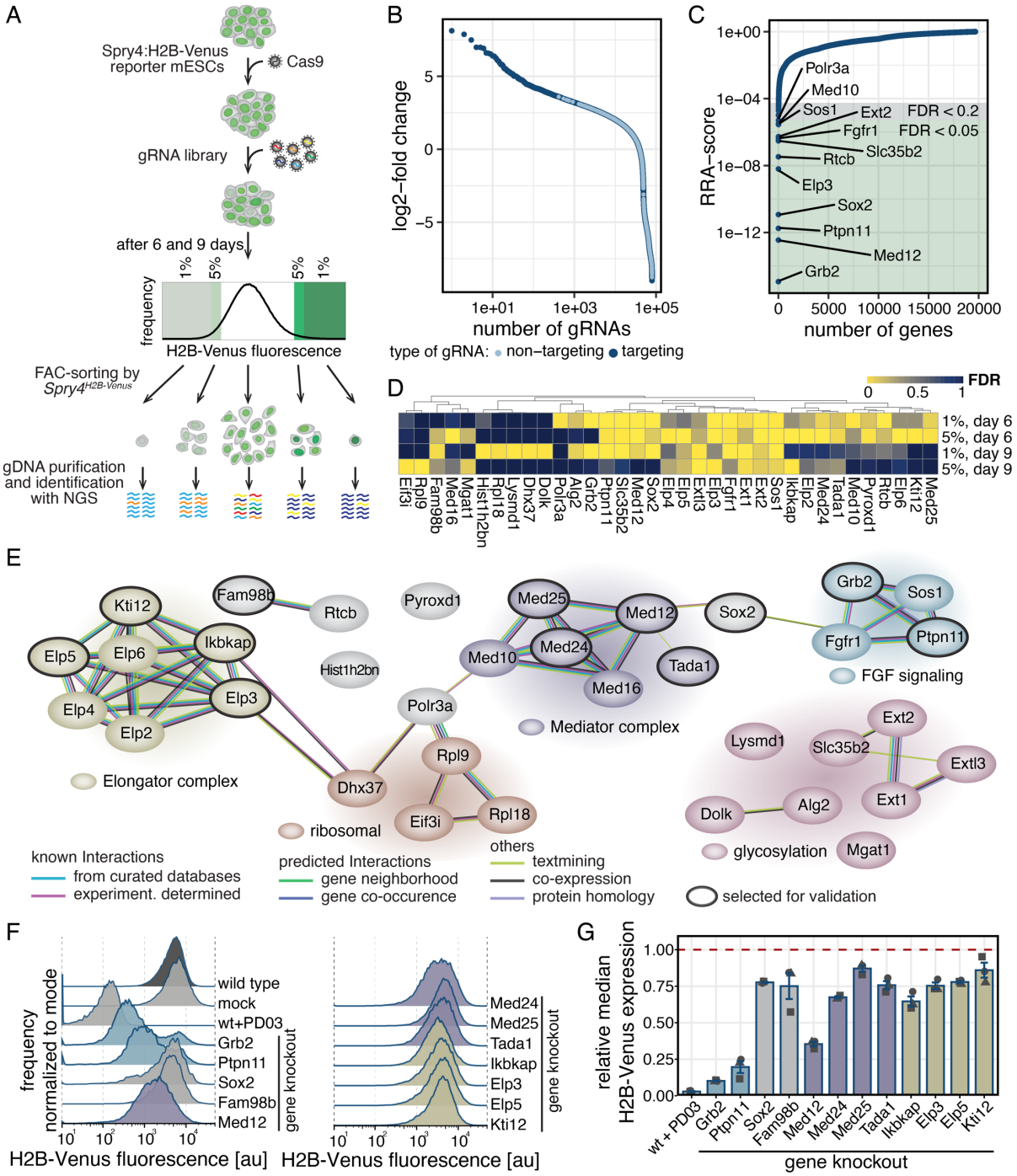

Fig. 1: Genome-wide CRISPR knockout screen reveals positive regulators of Sprouty4 expression.

A Schematic of the pooled CRISPR knockout screen. Cas9-expressing *Sprouty4*$^{H2B\text{-}Venus/+}$ reporter cells were transduced with a genome-wide gRNA library targeting protein-coding genes (Doench et al., 2016). Cells with in- or decreased fluorescence were flow sorted 6 or 9 days after transduction, and gRNAs enriched in sorted populations identified by sequencing.

B, **C** Enrichment of gene-targeting (dark blue) and control gRNAs (light blue) in cells sorted for the lowermost 1% of H2B-Venus signal 6 days after gRNA transduction, displayed as log2-fold change (B) or RRA score of corresponding genes (C). Green and gray background in (C) indicates FDR < 0.05 and < 0.2, respectively.

159 **D** Hierarchical clustering of gene perturbations leading to reduced *Spry4*$^{H2B\text{-}Venus}$ expression (FDR ≤
160 0.05 in at least one condition or FDR ≤ 0.2 in at least two conditions).
161 **E** Protein interaction network of genes shown in (D) based on String-DB. Background colors of genes
162 and gene clusters were manually assigned based on classification by functional similarity.
163 **F**, **G** H2B-Venus expression in *Spry4*$^{H2B\text{-}Venus/+}$ reporter cells upon knockout of selected candidate genes
164 6 d after transfection. (F) shows histograms of one representative experiment, (G) shows mean ± SEM
165 of median H2B-Venus expression from N = 3 independent experiments. $p < 0.05$ for wild type vs. *Elp3*,
166 *Elp5*, *Fam98b*, *Ikbkap*, *Kti12*, *Med25* or *Tada1* knockouts; $p < 0.01$ for wild type vs. *Grb2*, *Med12*,
167 *Med24*, *Ptpn11*, *Sox2* knockouts or PD03-treated cells (Benjamin-Hochberg-adjusted, one-sided,
168 paired t-test).
169
170 We next sought to use our screen to identify negative regulators of *Spry4* expression, by
171 looking at perturbations that led to increased reporter expression (Fig. 1A, right side of
172 histogram). Also here, gene-targeting gRNAs were enriched over control guides in the sorted
173 fractions (Fig. 2 Supp 1A-D, Supp Table 1). Ordering according to RRA-scores revealed up to
174 12 and 24 genes with FDR values of ≤ 0.05 and ≤ 0.2, respectively in each of the conditions
175 (Fig. 2A, Fig. 2 Supp 1E-G, Supp Table 1). Using the same criteria as for the positive
176 regulators, we compiled a list of 29 potential negative regulators of *Spry4* transcription (Fig.
177 2B). Analysis with String-DB again showed that many of these hits were highly connected and
178 associated with specific molecular functions (Fig. 2C). A large group of genes encoded
179 proteins that localized to mitochondria, or were otherwise associated with mitochondrial
180 functions. Several genes had signaling functions: *Lztr1* is a negative regulator of RAS-MAPK
181 and hence FGF signaling, in line with the strong representation of genes promoting FGF
182 signaling amongst the positive regulators of *Spry4* expression. We detected four genes that
183 were related to mTOR signaling (*Tsc1*, *Tsc2*, *Flcn*, and *Lamtor*). Finally, we found a big group
184 that contained genes involved in chromatin modification and transcription, amongst them three
185 genes encoding SWI/SNF related proteins. Thus, similarly to the collection of positive hits
186 identified above, our screen yields both signaling and transcriptional regulators that negatively
187 control *Spry4* expression. To select hits for validation, we focused on genes associated with
188 mTOR signaling, because these genes have also been implicated in the maintenance of
189 pluripotency (Betschinger et al., 2013; M. Li et al., 2018; Villegas et al., 2019). We also
190 included *Lztr1* as an FGF signaling gene, and *Smarcc1* as a representative of the group of
191 chromatin modifiers. Knockout of all six individual candidate genes with single gRNAs led to
192 an increase of mean *Spry4*:H2B-Venus fluorescence levels in reporter cells. The effect of
193 knocking out the mTOR signaling genes was stronger than that of knocking out *Lztr1* or
194 *Smarcc1*, and almost doubled reporter expression levels compared to mock-transfected cells
195 (Fig. 2D, E).

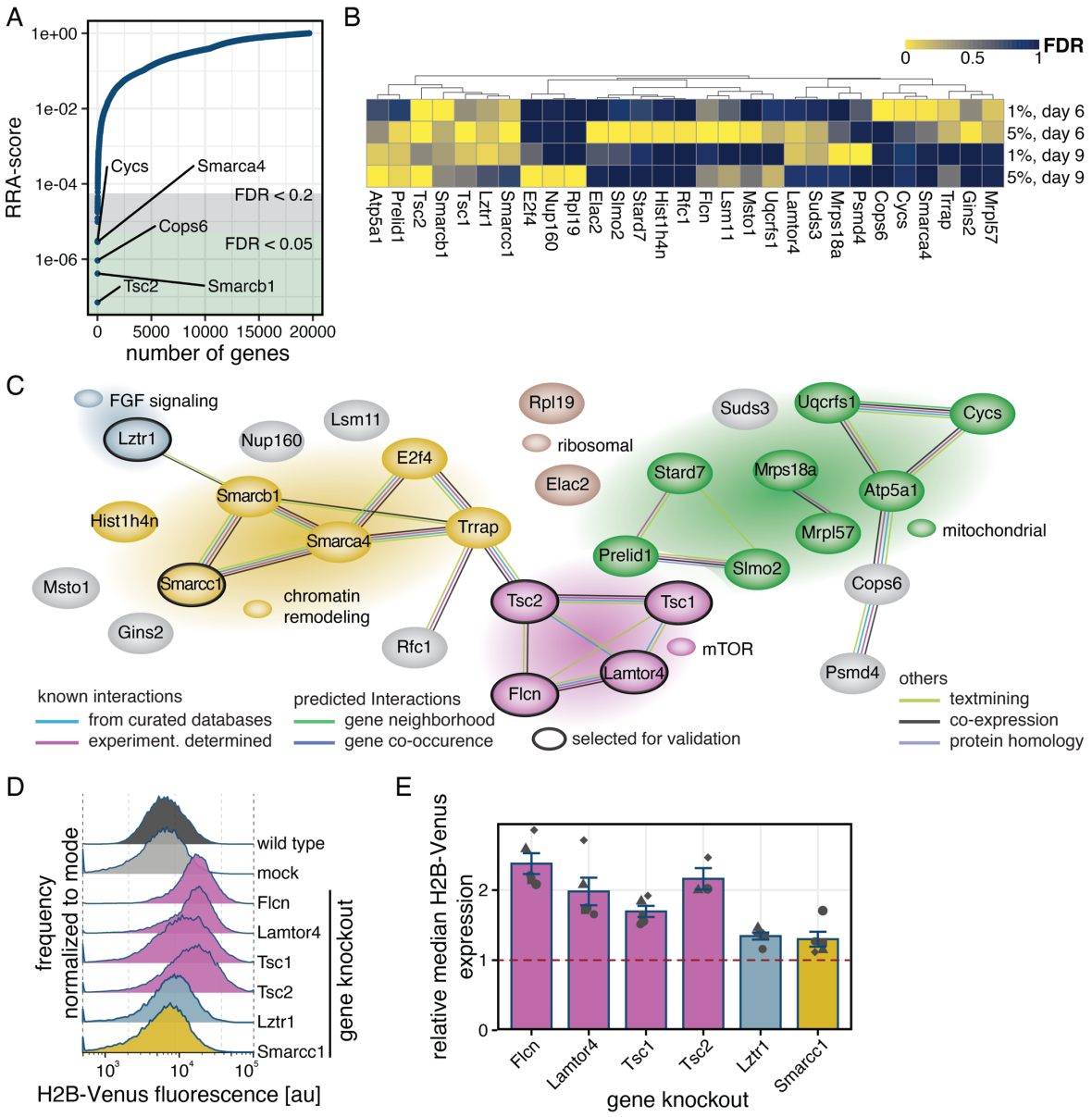

Fig. 2: Genome-wide CRISPR knockout screen reveals negative regulators of Sprouty4 expression.

A RRA scores of genes corresponding to gRNAs enriched in cells sorted for the topmost 1% of H2B-Venus signal on day 6 after gRNA transduction.

B Hierarchical clustering of gene perturbations leading to increased *Spry4*$^{H2B\text{-}Venus}$ expression (FDR ≤ 0.05 in at least one condition or FDR ≤ 0.2 in at least two conditions).

C Protein interaction network of genes shown in (B) based on String-DB. Background colors of genes and gene clusters were manually assigned based on classification by functional similarity.

D, **E** H2B-Venus expression in *Spry*$^{H2B\text{-}Venus/+}$ reporter cells upon knockout of selected candidate genes 6 d after transfection. (D) shows histograms of one representative experiment, (E) shows mean ± SEM of median H2B-Venus expression, N ≥ 3 independent experiments. $p < 0.05$ for mock-transfected wild type vs. *Smarcc1* knockout; $p < 0.01$ for mock-transfected wild type vs. all other knockouts (Benjamin-Hochberg-adjusted, one-sided, paired t-test).

Med12 regulates gene expression in mESCs independently from pluripotency-related signaling pathways

We then wanted to know how the signaling and transcriptional regulators identified in the CRISPR-screen were functionally related. We focused on *Med12*, since of all transcriptional regulators, it had the strongest effect on *Spry4* reporter expression. Furthermore, MED12 is a component of Mediator's kinase module which could couple the activities of specific signaling systems to transcriptional activity (Lynch et al., 2020; Rocha et al., 2010). To analyze *Med12* functions in mESCs, we first generated monoclonal *Med12*-mutant cell lines. We removed part of exon 7, a region that was also targeted by sgRNAs used in the CRISPR-screen, and confirmed the loss of MED12 protein expression by immunoblotting (Fig. 3 Supp 1A, B). *Med12*-mutant cells grew normally in both serum + LIF and 2i + LIF medium, and showed a reduced increase in *Spry4* reporter expression upon switching from 2i + LIF to the N2B27 base medium (Fig. 3 Supp 1C, D). ppERK levels were indistinguishable between wild-type and *Med12*-mutant lines (Fig. 3 Supp 1E, F), indicating that reduced *Spry4* reporter expression is not due to deregulated FGF/ERK signaling.

To assess global gene expression differences between wild-type and *Med12*-mutant cells, we performed bulk RNA sequencing of cells in 2i medium and upon 24 h of differentiation in N2B27 (Fig. 3A). Principal component analysis separated samples in pluripotency and differentiation medium along PC1 (32.1% of variance), and wild-type and *Med12*-mutant cells along PC2 (16.8% of variance, Fig. 3B). Fewer genes were differentially expressed between pluripotency conditions and 24 h in N2B27 in *Med12*-mutant compared to wild-type cells. Most genes that were differentially expressed in the mutant were also differentially expressed in the wild type (Fig. 3C, left, Supp Table 2). When comparing between wild-type and *Med12*-mutant cells within each culture condition, we found that more genes were differentially expressed between the two genotypes in N2B27 than in 2i (Fig. 3C, right, Supp Table 2). Thus, loss of *Med12* impairs gene expression changes at the exit from pluripotency. *Med12* has a closely related paralogue named *Med12l*. *Med12l* expression was upregulated in *Med12*-mutant cells (Fig. 3 Supp 2A), and *Spry4* reporter expression in *Med12*-mutant lines could be further reduced by simultaneously knocking-out *Med12l* (Fig. 3 Supp 2B). Thus, it is possible that *Med12l* partially compensates for loss of *Med12* function in the mutant lines.

Exit from pluripotency is regulated by the interplay of a set of signaling systems, such as mTOR, Notch, Wnt, and FGF (Betschinger et al., 2013; Kalkan et al., 2019; Ying et al., 2008). We next asked if gene expression downstream of any of these signaling systems was affected by loss of *Med12*, using previously defined sets of target genes specific for each signaling system (Lackner et al., 2021). A strong expression change of such a set of target genes

245 between wild type and mutant cells can be considered a footprint of the perturbation of the
246 corresponding signaling system. In *Med12* mutant cells, this gene expression footprint was
247 strongest for mTOR target genes, less pronounced for Notch and Wnt target genes, and
248 virtually absent for FGF target genes (Fig. 3D). We functionally tested the relationship between
249 *Med12* and mTOR signaling by knocking out the mTOR signaling genes *Flcn*, *Lamtor4*, *Tsc1*
250 and *Tsc2* in *Med12*-mutant *Spry4*$^{H2B\text{-}Venus/+}$ cells. Similarly to the situation in the wild type,
251 knockout of these genes led to increased reporter expression, albeit from a lower baseline
252 level (Fig. 3E). Therefore, *Med12* regulates *Spry4* expression independently from mTOR
253 signaling. In addition to mTOR signaling genes and Mediator subunits, our CRISPR screen
254 revealed a large number of genes involved in FGF signal transduction, but the footprinting
255 analysis suggested that FGF inputs into gene expression were independent from *Med12*. To
256 further corroborate this result, we generated *Med12* mutations in the background of an *Fgf4*-
257 mutant mESC line, which allowed us to specifically analyze the effects of FGF signaling upon
258 the switch from pluripotency to differentiation medium. We wanted to focus on immediate gene
259 expression changes triggered by FGF signaling, and therefore analyzed gene expression
260 changes by bulk RNA-sequencing after 6 h of transfer into N2B27 medium with or without
261 addition of exogenous FGF (Fig. 3F). Again, principal component analysis showed that cells
262 in pluripotency and differentiation medium were separated along PC1 (33.2% of variance),
263 and wild-type and *Med12*-mutant cells separated along PC3 (9.3% of variance), both when
264 analyzing independent *Med12*-mutant clonal cell lines as well as experimental replicates
265 (Fig. 3G). If expression of FGF target genes was generally dependent on *Med12,* we would
266 expect that their fold-change is lower in *Med12*-mutant compared to wild-type cells. However,
267 when plotting the fold expression-change for each gene upon 6 h of FGF stimulation for wild-
268 type versus *Med12*-mutant cells, we found that the majority of genes were induced to a similar
269 degree in both genotypes (2006 genes), while only 926 and 935 genes were differentially
270 expressed in the wild-type or the *Med12*-mutant only (Fig. 3H, Supp Table 3). Furthermore,
271 the ratios of fold-change values of FGF target genes between *Med12*-mutant and wild-type
272 cells showed a unimodal distribution with a mode of 1.068 for downregulated and 0.927 for
273 upregulated genes (Fig. 3J). While this slight deviation of the mode from 1 leaves open the
274 possibility that *Med12* influences their expression magnitude, overall these results argue
275 against a strong and specific role of *Med12* in the regulation of FGF target genes.

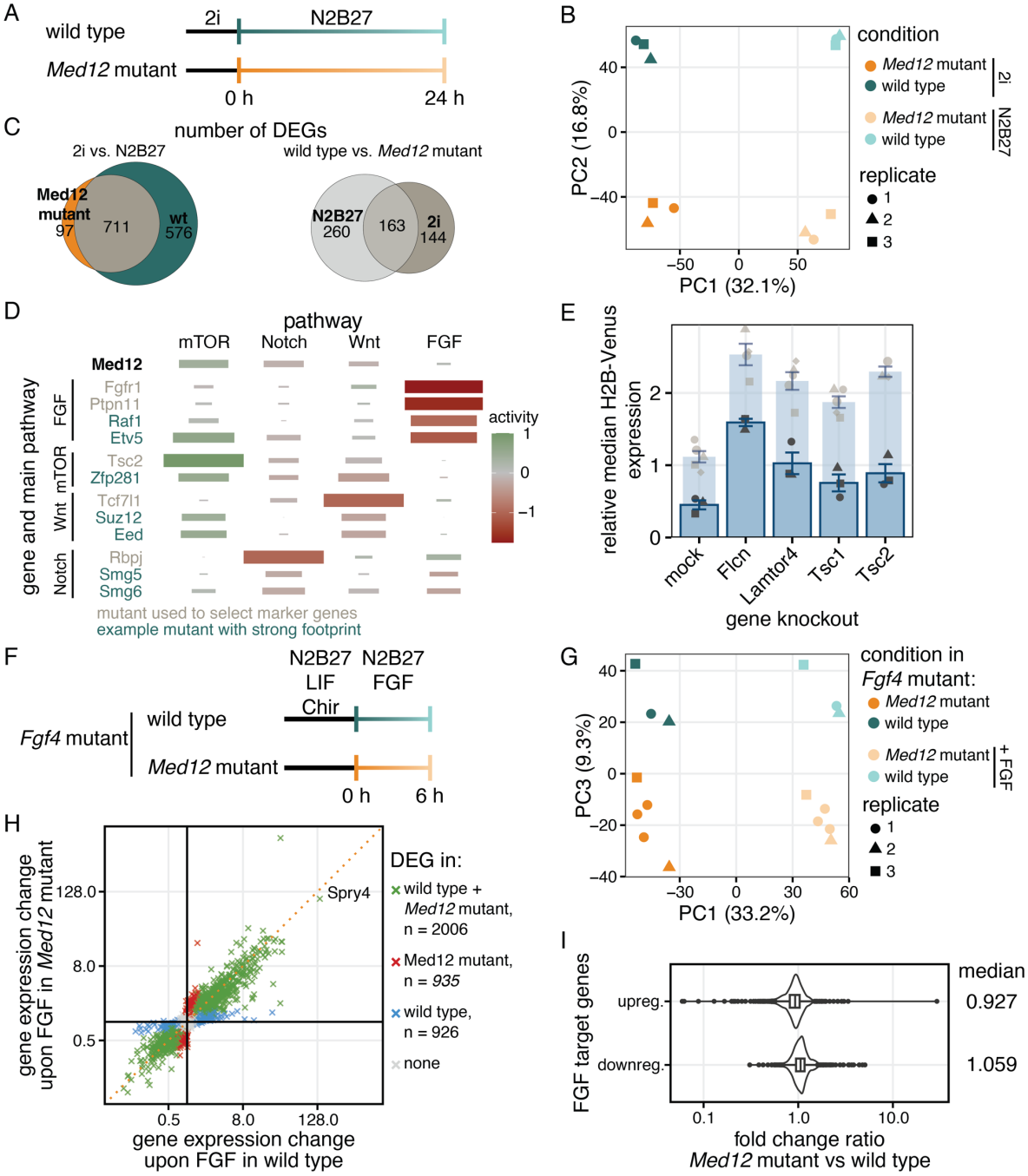

Fig. 3: *Med12* affects gene expression independently of pluripotency related signaling systems.
A Schematic of experiment to identify *Med12*-regulated genes by bulk RNA sequencing.
B Principal component analysis transcriptomes from (A).
C Euler-diagram showing the number differentially expressed genes (log2-fold change > |1|, adjusted p-value < 0.01) in bulk transcriptomes. Left panel compares genes differentially expressed upon 24 h of differentiation between *Med12*-mutant and wild-type cells, right panel compares genes differentially expressed upon loss of *Med12* between N2B27 and 2i.
D Expression footprint analysis using a set of 50 marker genes per pathway defined in (Lackner et al., 2021). Top row shows footprint of *Med12*-mutant cells. Lower rows show expression footprints of mutants from Lackner et al., 2021, for comparison. Gray: Mutants that were used to select marker genes. Green: Independent example mutants that show a strong and specific footprint of one of the

288 pathways. Tile color indicates relative pathway activity, tile size indicates spearman correlation of
289 footprint genes with pathway-defining mutants.
290 **E** Median H2B-Venus fluorescence upon mutation of mTOR related genes in *Med12*-mutant *Spry4*$^{H2B-}$
291 $^{Venus/+}$ cells, normalized to H2B-Venus expression in *Med12* wild-type cells. Median H2B-Venus
292 fluorescence upon mutation of mTOR related genes in *Med12* wild-type cells is reproduced from Fig.
293 2E for comparison (light blue). Error-bars indicate SEM, points individual replicates, N ≥ 3 independent
294 experiments.
295 **F** Schematic of experiment to test *Med12*-dependency of FGF target genes by RNA sequencing.
296 **G** Principal component analysis transcriptomes from (F). PC2 (not shown; 12.8% of variance) separated
297 experimental replicates from each other.
298 **H** Gene expression changes and number of significantly differentially expressed genes (adjusted p-
299 value < 0.01) upon FGF4 stimulation in wild-type versus *Med12*-mutant cells. Dotted orange line
300 indicates the unity line.
301 **I** Ratio of fold changes for FGF target genes between wild-type and *Med12*-mutant cells, for up- (top)
302 and downregulated genes (bottom). FGF target genes were defined as having a log2-fold change in
303 wild-type cells upon FGF4 stimulation > |1| and an adjusted p-value < 0.05.
304

305 *Med12* regulates naïve pluripotency

306 We then asked if altered gene expression in the *Med12* mutants had any functional
307 consequences. To probe exit from naïve pluripotency, we performed a colony formation assay
308 (Kalkan et al., 2017), where we differentiated cells in N2B27 for 48 h, followed by seeding at
309 clonal density in 2i + LIF medium (Fig. 4A). Because we grew cells in the presence of LIF
310 before transfer into N2B27, wild-type cells still formed a large number of pluripotent colonies
311 (Lackner et al., 2021). In *Med12*-mutant cells in contrast, the number of pluripotent colonies
312 was significantly reduced. (Fig. 4B, left, Fig. 4 Supp 1A, Supp Table 4). To test how this
313 phenotype related to FGF signaling, we carried out the same colony differentiation assay in
314 an *Fgf4* mutant background. When differentiated for 48 h in N2B27, *Med12* wild-type and
315 mutant cells formed a similar number of colonies upon transfer to pluripotency medium. Upon
316 supplementation of N2B27 with FGF4, the number of pluripotent colonies formed by *Fgf4;*
317 *Med12* double mutant cells was much reduced, both compared to the *Fgf4* single mutant
318 supplemented with FGF4, and the *Fgf4; Med12* double mutant in the absence of FGF4 (Fig.
319 4B, right, Fig. 4 Supp 1B). Thus, this experiment corroborates our conclusion from the
320 transcriptomic analysis that Med12 cooperates with FGF signaling at the exit from
321 pluripotency.
322 The ability to form pluripotent colonies in the colony formation assay depends on a cell's
323 pluripotency state at the beginning of the differentiation period, and its ability to react to
324 changing culture conditions. We used our bulk RNA sequencing data comparing wild-type and

325 *Med12*-mutant cells after 24 h in N2B27 to evaluate which of these properties were affected
326 upon loss of *Med12*. We first determined differentiation delays of the two genotypes using a
327 published high time-resolution reference dataset (Lackner et al., 2021). Surprisingly, this
328 analysis indicated that *Med12*-mutant cells differentiated more slowly than the wild-type (Fig.
329 4C). This could be a consequence of stronger expression of naïve genes in pluripotency
330 conditions, or reflect slower downregulation of these genes in N2B27 in the *Med12* mutant. To
331 distinguish between these possibilities, we plotted the expression levels of 7 selected
332 pluripotency marker genes in 2i and after 24 h in N2B27 in wild-type versus *Med12*-mutant
333 cells. In this plot, data points above and below the unit line indicate higher and lower
334 expression in the mutant relative to the wild type, respectively, and the slope of the connecting
335 line between expression in 2i and N2B27 indicates the dynamics of down-regulation (Fig. 4D,
336 left). We found that in 2i medium, all marker genes were less strongly expressed in the mutant
337 compared to the wild type. Furthermore, their slopes were consistently smaller than one (Fig.
338 4D). Such a systematic reduction in the slope of downregulation was also observed when we
339 analyzed the top 100 downregulated genes in wild-type or *Med12*-mutant cells (Fig. 4E).
340 These findings suggest that *Med12*-mutant cells both have impaired pluripotency gene
341 expression in 2i, as well as a reduced ability to react to changing culture conditions. In the
342 colony formation assay, cells need to re-establish pluripotency gene expression. We therefore
343 surmise that the reduced colony formation capacity of *Med12*-mutant cells in the colony
344 formation assay is dominated by their reduced ability to react to changing culture conditions.

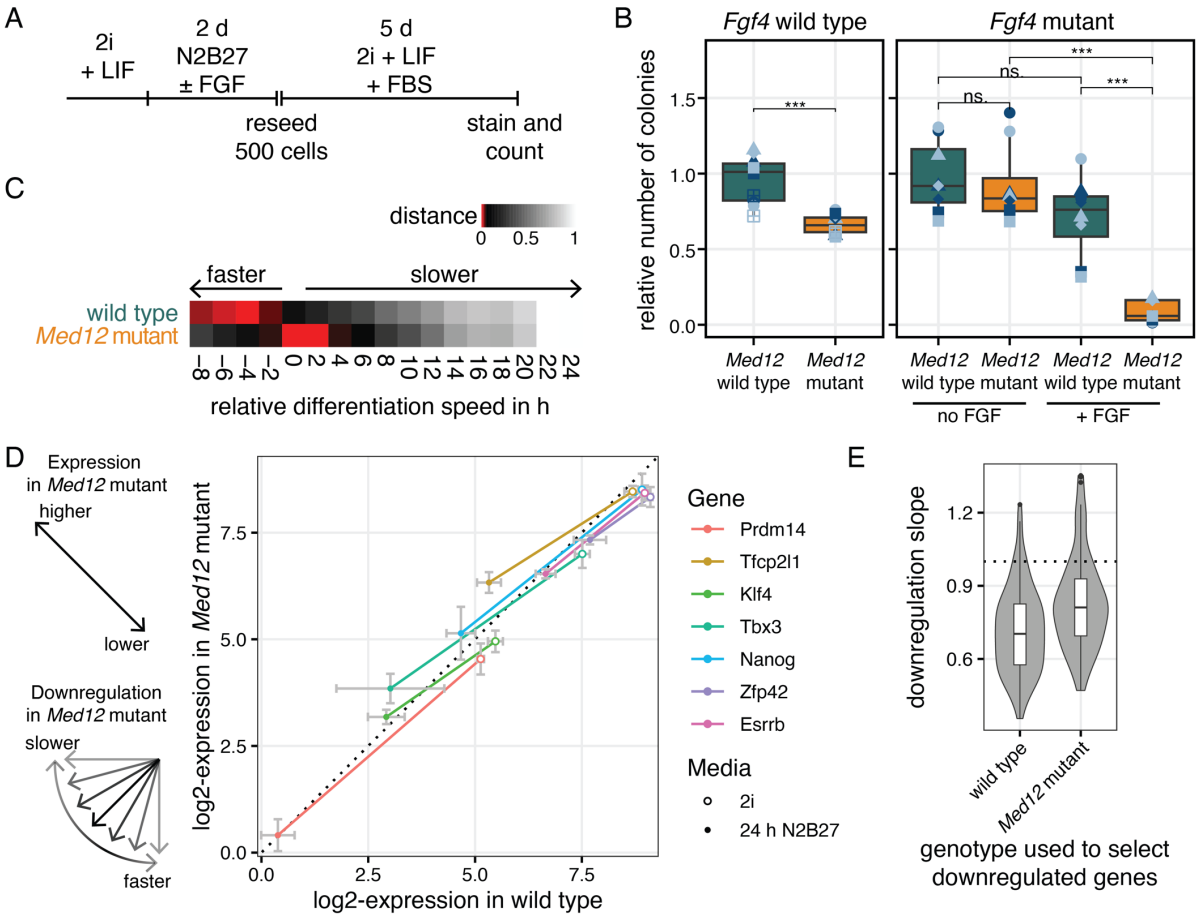

Fig. 4: Mutation of *Med12* affects the exit of pluripotency.

A Experimental approach to determine clonogenicity of *Med12*-mutant and wild-type cells. 2i + LIF was supplemented with FBS to support growth of *Fgf4*-mutant cells after reseeding.

B Number of colonies after treatment as indicated in (A) for both wild-type and *Med12*-mutant cells in an *Fgf4* wild-type (left) and *Fgf4* mutant background with and without supplementation with 10 ng/µL FGF4 (right). N ≥ 4 independent experiments, same symbols in different colors indicate technical replicates within an independent experiment. ns indicates p ≥ 0.05, *** indicates p ≤ 0.001, paired Wilcoxon signed rank test.

C Estimation of differentiation delay in wild-type and *Med12*-mutant cells, relative to a published time resolved gene expression dataset (Lackner et al., 2021). Plot shows the normalized Euclidean distance of the expression of naïve marker gene panel (*Prdm14*, *Tfcp2l1*, *Klf4*, *Tbx3*, *Nanog*, *Zfp42*, *Esrrb*) to the reference dataset. The negative delay values for our wild-type cells likely reflect small differences in experimental design compared to the study by (Lackner et al., 2021).

D Expression of naïve pluripotency marker genes in 2i (open circles) and after 24 h differentiation in N2B27 (dots) in wild-type versus *Med12*-mutant cells. Relative expression values shown as log2(TPM), error bars indicate standard deviation.

E Distribution of downregulation slopes determined as in **D** for the 100 genes with the strongest negative fold-change in wild-type (left) and *Med12*-mutant cells (right). Bar indicates median, boxes indicate 25th and 75th percentile.

Transition between embryonic and extraembryonic identities is buffered against loss of *Med12*

We next sought to further probe the role of *Med12* in an experimental system where the doxycyclin-induced expression of GATA factors brings ground state pluripotent cells into an ICM-like state, from which they can differentiate towards the Epi identity marked by NANOG expression, or the PrE identity marked by the expression of endogenous GATA factors and SOX17 (Fig. 5A; Schröter et al., 2015). We used PiggyBac transgenesis to establish new cell lines carrying inducible GATA6-mCherry constructs, and mutated *Med12* in this background to determine if it is required for PrE differentiation. After an 8 h doxycycline pulse followed by 20 h of differentiation in N2B27 medium, a mix of SOX17-positive PrE cells and NANOG-positive Epi cells differentiated irrespective of *Med12* status, but the fraction of PrE cells was lower, and that of Epi cells was higher in mutant compared to wild-type cultures (Fig. 5B, C). This difference in ratios was maintained even upon supplementation of exogenous FGF during the differentiation phase, suggesting that the lowered PrE differentiation propensity upon loss of *Med12* is not due to lowered FGF signaling in the mutant cultures (Fig. 5 Supp 1A).

PrE differentiation requires the expression of inducible GATA factors above a threshold level (Schröter et al., 2015). We therefore assessed transgene induction levels in *Med12* mutant cells, and found that they were reduced in independent clonal inducible lines (Fig. 5D). To test if *Med12* mutant cells had an altered GATA induction threshold for PrE differentiation, we performed time-lapse imaging of inducible GATA6-mCherry expression followed by fixation and staining for fate markers (Schröter et al., 2015). We attempted to equalize induction levels by reducing the induction time in wild-type cells to 4 h, while inducing *Med12*-mutant cells for 8 h in 2i + LIF medium. The mutant cells showed a longer delay between doxycycline addition and the appearance of GATA6-mCherry fluorescence, and GATA6-mCherry expression levels rose more slowly than in the wild type. Furthermore, GATA6-mCherry levels continued to rise for approximately 2 h after doxycycline removal in wild-type but not in *Med12*-mutant cells (Fig. 5E, Supp Movie 1). These altered induction dynamics point to a critical role of *Med12* for efficient transgene expression.

Connecting inducible GATA expression with differentiation outcome in individual cells revealed that low and high inducible GATA6-mCherry expression in *Med12* mutants were associated with Epi and PrE differentiation, respectively, similar to the situation in wild-type cells (Fig. 5F, G; Schröter et al., 2015). We applied receiver operating characteristics to test how well differentiation could be predicted based on a GATA6-mCherry expression threshold, and to determine the value of an optimal threshold (Fawcett, 2006). GATA6-mCherry expression levels had similar predictive power for differentiation outcome in wild-type and

Med12-mutant cells as judged by plotting the area under the curve (AUC) over time (Fig. 5H). When comparing optimal threshold values, we found that these tracked overall GATA6-mCherry expression levels and were thus slightly lower in *Med12*-mutant cells (Fig. 5I). This indicates that altered proportions of Epi and PrE cells upon loss of *Med12* are largely due to reduced transgene induction levels and not to a reduced ability for PrE differentiation. This conclusion was further supported by flow sorting wild-type and Med12-mutant cells with high GATA6-mCherry expression levels (Fig. 5 Supp 1 C, D). Disruption of cell-cell interactions upon sorting and reseeding resulted in low PrE differentiation in N2B27 medium (Raina et al., 2021), but supplementation of exogenous FGF4 rescued PrE differentiation to similarly high levels in both wild-type and *Med12*-mutant cells (Fig. 5 Supp 1 D, E). Taken together, these experiments suggest that although *Med12* plays important roles for the efficient expression of individual genes, the transition between embryonic and extraembryonic identities is to a large degree buffered against loss of *Med12*.

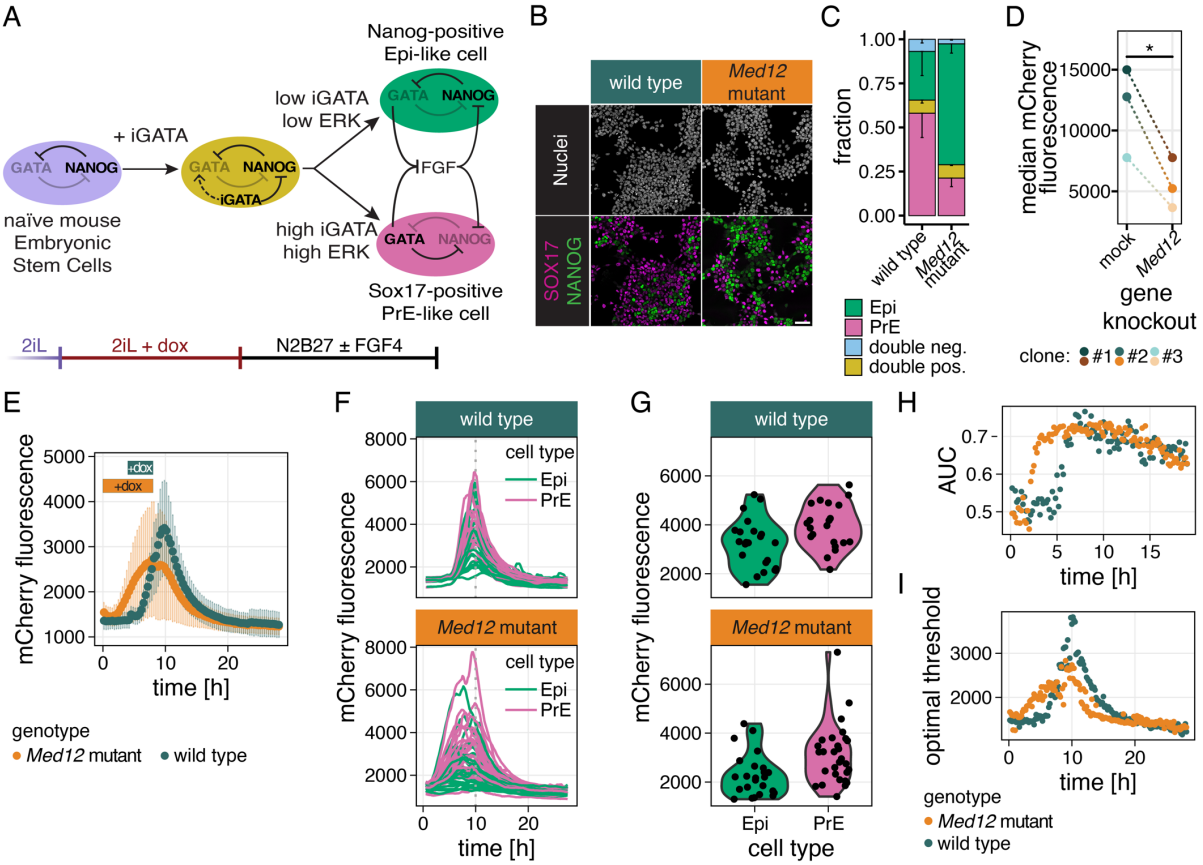

Fig. 5: Transition between embryonic and extraembryonic identities is buffered against loss of *Med12*.

A Schematic of experimental approach to model differentiation of mESCs towards epiblast and primitive endoderm via GATA induction.

B Immunostaining for the Epi-marker NANOG (green) and the PrE marker SOX17 (magenta) after 8 h of GATA6 induction followed by 20 h of differentiation in wild-type and *Med12*-mutant cells. Scale bar: 50 µm.

421 **C** Quantification of cell type proportions after differentiating wild-type and *Med12*-mutant cells as in (B).
422 N = 3, n > 1100 cells per replicate, error bars indicate SEM.
423 **D** Median Gata6-mCherry fluorescence upon 8h dox induction in three independent clonal GATA6-
424 mCherry inducible cell lines 7 days after transfection with control or *Med12*-targeting gRNAs. * indicates
425 $p \leq 0.05$, paired student's t-test.
426 **E** Quantification of Gata6-mCherry expression dynamics from time-lapse movies during induction and
427 differentiation. Boxes indicate induction times (8 h for *Med12* mutant, 4 h for wild type). Error bars
428 indicate SD. One out of N = 5 replicates shown, n > 300 cells per time point.
429 **F** Same experiment as in (E), but showing Gata6-mCherry fluorescence in single cells. Trace color
430 indicates differentiation outcome determined by immunostaining (Epi: green; PrE: magenta).
431 **G** Gata6-mCherry fluorescence in single cells 2 h after the end of induction, plotted separately for
432 prospective Epi and PrE cells.
433 **H** Predictive power of GATA6-mCherry expression determined as Area Under the Curve (AUC) from
434 ROC-analysis.
435 **I** Optimal GATA6-mCherry threshold to predict differentiation outcome determined by Youden's J
436 statistic of ROC-analysis.
437 **F** - **I** Data from one representative experiment out of N = 3 replicates, n ≥ 45 cells per genotype.
438

439 Loss of *Med12* reduces biological noise

440 Finally, we performed single-cell sequencing to determine how Med12 shapes the global
441 transcriptional signature of PrE differentiation. Multiplexing and pooling of samples before
442 mRNA capture and library preparation allowed us to minimize batch effects, and to generate
443 sample replicates using independent *Med12* wild type and mutant cell lines (Fig. 6A). As in
444 previous experiments, we induced GATA transgenes for 4 h in wild-type and 8 h in *Med12*-
445 mutant cells, and started differentiation simultaneously in both genotypes by switching from 2i
446 + LIF medium to N2B27. In a UMAP representation of transcriptomes from all ten samples,
447 cells from pluripotency and differentiation conditions formed two coherent groups,
448 respectively. Within each of the groups, wild type and *Med12*-mutant cells segregated from
449 each other (Fig. 6B). Cells from differentiation conditions were negative for the Wnt/β-Catenin
450 target *Sp5* and positive for the differentiation marker *Dnmt3l*, while PrE markers *Sox17, Dab2*,
451 and *Cubn* and the Epi markers *Nanog* and *Fgf4* showed a mutually exclusive expression
452 pattern, indicative of the split between the two lineages (Fig. 6C). To evaluate the
453 consequences of loss of *Med12* in this experiment, we next analyzed pluripotency and
454 differentiation samples separately, and used principal component analysis as a means to
455 graphically preserve quantitative differences in gene expression between cells. In pluripotency
456 conditions, single cell transcriptomes from wild-type and *Med12*-mutant cells were clearly
457 separated, demonstrating that loss of *Med12* leads to a globally consistent shift of gene

458 expression state (Fig. 6D). Consistent with our results from bulk RNA sequencing, expression
459 levels of the pluripotency genes *Klf4*, *Zfp42*, and *Tbx3* were reduced in the mutant cells,
460 whereas levels of *Prdm14*, *Nanog*, *Esrrb*, and *Tcf21l1* were similar between the two genotypes
461 (Fig. 6E). Next, we exploited our multiplexed dataset to ask if loss of *Med12* changes mRNA
462 levels in cells. In pluripotency conditions, the number of mRNAs captured from wild-type and
463 *Med12*-mutant cells was not significantly different (median number of UMIs 24437 and 23806,
464 respectively). Differentiation resulted in an increased number of captured mRNAs in both
465 genotypes, with wild-type cells expressing significantly more mRNAs than *Med12* mutants
466 (median number of UMIs 28227 and 25649, respectively, Fig. 6E). This suggests that *Med12*
467 enhances global transcriptional output during differentiation.
468 We then asked how loss of *Med12* affected the separation between Epi and PrE identities. To
469 consistently identify Epi and PrE cells across genotypes, we integrated the five differentiated
470 samples and clustered them to separate two major groups across the integrated dataset (Fig.
471 6G). In principle component space, these two groups were separated along PC1 (Fig. 6G).
472 Cluster 0 was characterized by the expression of PrE marker genes such as *Gata6*, while
473 cluster 1 expressed Epi markers such as *Nanog* (Fig. 6 H, Supp Table 5). The proportions of
474 the two cell types captured by these clusters differed with *Med12* genotype: In the two wild-
475 type cell lines, 60% and 77% of all cells fell into the PrE cluster 0, whereas this cluster
476 contained only between 35% and 42% of all cells in the *Med12* mutants (Fig. 6I). We then
477 used the cell type annotation based on this clustering approach to ask how similar the changes
478 in gene expression profiles were between wild-type and *Med12*-mutant cells upon
479 differentiation towards either of the two lineages. We first focused on genes that had a log2
480 fold change ≥ 0.5 between pluripotency and differentiation in wild-type cells. The fold-changes
481 of these genes in the mutant showed a unimodal distribution in all four conditions (up- and
482 downregulation, Epi and PrE differentiation), indicating that *Med12* is not required for the
483 regulation of specific gene modules during differentiation (Fig. 6J). This conclusion was
484 supported by plotting the fold-change of all genes upon differentiation against each other for
485 wild-type and mutant cells (Fig. 6 Supp 1 A, B). When comparing the top differentially
486 expressed genes between wild type and mutant in pluripotency conditions as well as in the
487 Epi and PrE clusters, we found that many of these genes were differentially expressed in all
488 three states (Fig. 6 Supp 1C, Supp Table 6). This suggests that loss of *Med12* does not
489 prevent differentiation, but rather results in gene expression changes that are shared between
490 cell states.
491 Despite not regulating specific differentiation-associated gene modules, loss of *Med12* could
492 still influence the efficiency of lineage separation. In the PCA plot in Fig. 6E, we noted that
493 transcriptomes of Epi and PrE cells were separated more clearly in *Med12*-mutant compared
494 to wild-type cultures. The Jaccard index is a quantitative measure for the separation of clusters

495 in single cell sequencing data (Tang et al., 2021). We therefore computed the Jaccard index
496 for clustering of 100 random subsets of each differentiated sample without integration
497 (Materials and Methods). The average Jaccard index was higher in *Med12*-mutant samples
498 compared to wild type, demonstrating that loss of *Med12* indeed leads to a better
499 transcriptional separation of clusters (Fig. 6K). This could be a consequence of different
500 transgene induction dynamics between genotypes, or result from a reduction of cellular
501 plasticity upon loss of *Med12.* Consistent with differences in plasticity, wild-type cells, but not
502 *Med12*-mutant cells, showed a long tail of the Jaccard index distribution indicating the
503 presence of a population of cells that explore transcriptional space beyond the main clusters.
504 As an alternative measure, we used VarID2 (Rosales-Alvarez et al., 2023) to test if biological
505 noise levels were changed upon loss of *Med12*. This analysis revealed reduced noise levels
506 in *Med12* mutants in all three differentiation states, with the strongest changes in pluripotency
507 and in Epi cells (Fig. 6L). Taken together, these results indicate that loss of *Med12* results in
508 overall lower transcriptional output and decreased noise. These effects may result in reduced
509 cellular plasticity during lineage transitions, which can enhance separation between lineages.

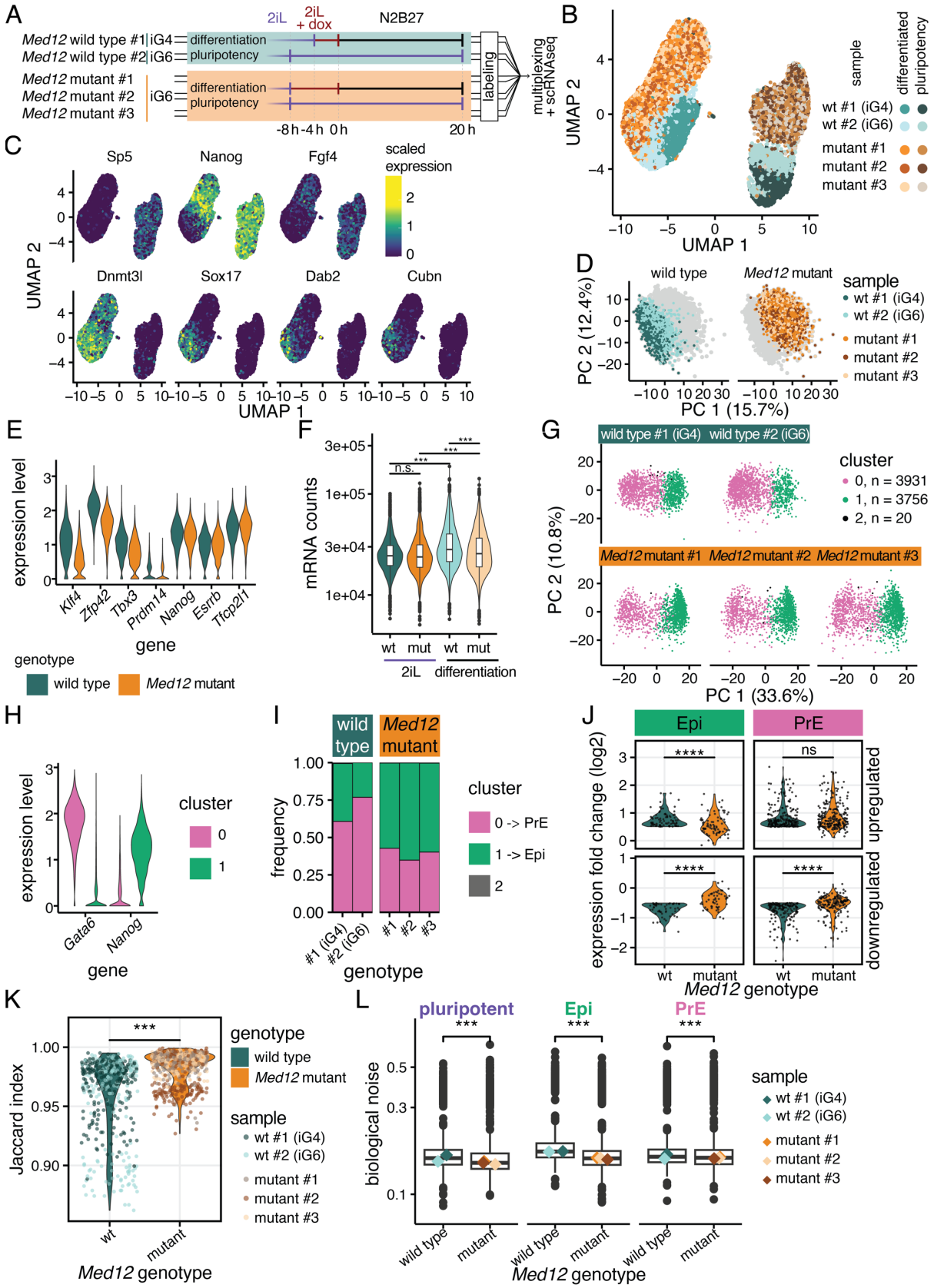

Fig. 6: Role of *Med12* in PrE differentiation.

A Schematic of the single cell RNA sequencing experiment to compare single cell transcriptional signatures between wild-type and *Med12*-mutant cells in pluripotency and upon PrE differentiation. Replicates were generated by including two *Med12* wild-type lines carrying inducible GATA4- or

515 GATA6-mCherry transgenes (iG4 and iG6), and three independent *Med12*-mutant cell lines derived
516 from the GATA6-mCherry inducible line. Doxycycline induction was 4 h and 8 h in wild-type and *Med12*-
517 mutant cells, respectively.
518 **B** UMAP plot of single cell transcriptomes from all 10 samples.
519 **C** Ln-scaled expression levels of selected marker genes projected onto the UMAP plot from (B).
520 **D** Principal component analysis of single cell transcriptomes from wild-type and *Med12*-mutant cells in
521 pluripotency conditions.
522 **E** Ln-transformed expression levels of same naïve pluripotency marker genes as in Fig. 4C,D.
523 **F** Number of detected mRNAs per cell in wild-type and *Med12*-mutant cells. ns indicates $p \geq 0.05$, ***
524 indicates $p \leq 0.001$, Bonferroni-adjusted Kolmogorov-Smirnov test.
525 **G** Principal component analysis and Louvain-clustering of single-cell transcriptomes from wild-type and
526 *Med12*-mutant cells after differentiation.
527 **H** Ln-transformed expression levels of the PrE-marker gene *Gata6* and the Epi-marker gene *Nanog* in
528 the differentiated samples split by cluster. Cluster 2 was excluded due to the small number of cells.
529 **I** Proportions of cell types, identified by clustering, in wild-type and *Med12*-mutant cells.
530 **J** Comparison of up- (top panels) and downregulated genes (bottom panels) in wild-type and *Med12*-
531 mutant cells upon differentiation from pluripotency to Epi (left) or PrE (right). Shown are genes with a
532 log2-change of expression > 0.5 in wild-type cells. ns indicates $p \geq 0.05$, **** indicates $p \leq 0.0001$,
533 paired Wilcoxon signed rank test.
534 **K** Jaccard index to assess cluster stability of wild-type and *Med12*-mutant cells. ns indicates $p \geq 0.05$,
535 *** indicates $p \leq 0.001$, Kolmogorov-Smirnov test.
536 For clarity, measurements from the two *Med12* wild-type and the three *Med12*-mutant lines were pooled
537 in panels E, F, J, and for the violin plot and statistical test in K.
538 **L** Biological noise determined for each cell state (pluripotency, Epi and PrE) and genotype (*Med12* wild
539 type and mutant) using VarID2 (Rosales-Alvarez et al., 2023). Medians for single clonal lines are
540 indicated as diamond. **** indicates $p \leq 0.0001$, Wilcoxon signed rank test. Bar indicates median, boxes
541 indicate 25th and 75th percentile.

Discussion

Here we use a *Spry4*$^{H2B\text{-}Venus}$ reporter to screen for regulators of developmental gene expression in pluripotent stem cells. This screen returned components of the FGF/ERK and the mTOR signaling systems that positively and negatively regulate reporter expression, respectively, as well as several members of the Mediator and Elongator complexes. Focusing on *Med12* we show that it cooperates with multiple signaling systems to regulate gene expression in pluripotent cells. Functional assays reveal that loss of *Med12* both reduces the ability to re-establish a naïve pluripotency gene expression program in colony forming assays, as well as the propensity to populate transition states in an epiblast-to-primitive endoderm differentiation paradigm. These phenotypes correlate with reduced noise in *Med12*-mutant cells. Together, these results suggest that *Med12* amplifies transcriptional changes in pluripotent cells, and thereby contributes to the maintenance of cellular plasticity during differentiation and lineage transitions.

Previous genome-wide screens have used retention of clonogenicity or the continued expression of pluripotency-associated reporter alleles in differentiation conditions as read-outs to identify regulators of pluripotency and lineage transitions (Betschinger et al., 2013; Kagey et al., 2010; M. Li et al., 2018; Villegas et al., 2019). In our study, the combination of a *Spry4*$^{H2B\text{-}Venus}$ allele with flow sorting constitutes a highly sensitive read-out that is focused on the activity of specific signaling systems in pluripotent cells, and reliably detects new regulators even if they have only small effect sizes. The screen's specificity shows in the strong representation of genes involved in the FGF/ERK signaling cascade, from genes that encode synthetases for FGF co-factors, over FGF receptors, to intracellular signaling genes. Surprisingly however, we did not find any sequence-specific transcription factors downstream of FGF/ERK signaling in our screen. This could be explained by the expression of multiple functionally redundant FGF/ERK signaling effectors in pluripotent cells, or through previously proposed transcription factor-independent regulation of RNA polymerase activity by ERK (Tee et al., 2014).

In addition to components of FGF and mTOR signaling systems, the screen returned several members of the SWI/SNF and the Mediator complexes. The core Mediator complex is thought to be required for the expression of most genes in eukaryotic genomes, but individual subunits have been suggested to regulate gene expression downstream of specific signaling systems such as the serum response network (Donner et al., 2010; Stevens et al., 2002), or Wnt (Rocha et al., 2010). However, when we tested this idea for *Med12*, we found that its loss did not phenocopy the effects of specific signaling perturbations. This finding suggests that previously reported functional connections, such as the link between *Med12* and Wnt signaling (Rocha et al., 2010), are strongly context-dependent.

577 *Med12* is a critical component of the Mediator-associated CDK8-module. In contrast to
578 pharmacological inhibition of CDK8 which has been reported to boost pluripotency similarly to
579 ERK signaling inhibition (Lynch et al., 2020), we find that loss of *Med12* leads to reduced
580 pluripotency. These opposing phenotypes indicate that MED12 has functions that are
581 independent from the CDK8-module (Aranda-Orgilles et al., 2016). This would also explain
582 why we did not detect any other CDK8-module components in our screen. Lynch et al. found
583 that maintenance of pluripotency required the presence of CDK8, but absence of its kinase
584 activity. Another possible explanation for the opposing phenotypes of CDK8 inhibition and
585 *Med12* loss-of-function therefore is that MED12 participates in assembling kinase-inactive
586 CDK8 complexes that support pluripotency.
587 *Med12*'s function to maintain pluripotency reported in the present work is supported by earlier
588 studies which found that MED12 and NANOG proteins interact, that MED12 and NANOG have
589 similar DNA-binding profiles, and that MED12 promotes *Nanog* expression (Apostolou et al.,
590 2013; Tutter et al., 2009). Several Mediator subunits, including *Med12*, have been identified
591 in a screen for pluripotency maintenance that focused on transcription and chromatin
592 regulators (Kagey et al., 2010). This study furthermore suggested that interactions between
593 Mediator and cohesin contribute to genome folding and efficient enhancer-promoter
594 interactions. When we probe *Med12* functions in lineage transitions, we find that *Med12*-
595 mutant cells show decreased transcriptional plasticity, which manifests in a slower
596 downregulation of pluripotency genes, a decreased ability to revert to naïve pluripotency in a
597 colony-forming assay, and a reduced tendency to populate transition states in the binary
598 decision between an epiblast and a primitive endoderm identity. We speculate that these
599 cellular phenotypes are a reflection of a reduced ability of *Med12*-mutant cells to reconfigure
600 the chromatin upon changing signaling environments. It is likely that the expression of
601 individual genes is differentially sensitive to the loss of *Med12*. This may be the reason why
602 expression from the *Sprouty4* locus, which is the most strongly upregulated gene upon acute
603 FGF stimulation, shows a particularly high sensitivity to loss of *Med12*. In line with this idea,
604 requirements of *Med12* for efficient induction are not exclusive to endogenous genes, but
605 extend to exogenous transgenes such as the inducible GATA6-mCherry construct used to
606 trigger primitive endoderm differentiation in our study. Surprisingly, such differential
607 quantitative defects in the regulation of single genes upon loss of *Med12* do not lead to strong
608 defects in acquiring early differentiated fates, such that transcriptomes of individual
609 differentiated cells are not systematically different from each other in *Med12*-mutant and wild-
610 type cells. This suggests that intracellular regulatory networks can buffer the composition of
611 cellular transcriptomes against variable transcription efficiencies.

612 # Acknowledgements

613 We thank Kristin Nowak for generating *Fgf4*-mutant E14tg2a mESC lines, members of the
614 Imig lab for help with lentivirus production, and the protein chemistry facility of the MPI
615 Dortmund for supply of LIF and enzymes for molecular biology. Michelle Marten provided
616 technical and organizational support for tissue culture and flow sorting throughout the project.
617 We thank members of the Schröter lab, the Department of Systemic Cell Biology, Jochen Imig
618 and Cristina Pina for critical discussions and feedback on earlier versions of the manuscript.

619 # Declaration of interest

620 The authors declare that they have no conflict of interest.

Materials and Methods

Cell culture

Routine culture of mESCs was performed at 37 °C with 5% CO_2 in either serum + LIF medium (ESL, composed of GMEM with 10% fetal bovine serum (FBS), 2 mM GlutaMAX, 1 mM sodium pyruvate, 0.1 mM b-mercaptoethanol and 10 ng/mL LIF), on 0.1% gelatine coated dishes, or in 2i + LIF medium on fibronectin coated dishes. 2i + LIF is N2B27 supplemented with 1 µM PD0325901 (SelleckChem), 3 µM CHIR99201 (Tocris) and 10 ng/ml LIF (protein chemistry facility, MPI Dortmund). N2B27 was prepared as a 1:1 mixture of DMEM/F12 and Neuropan Basal Medium (both from PAN Biotech), supplemented with 1X N2 and 1X B27 supplements, 1X L-Glutamax, 0.0025% BSA, and 0.2 mM ß-mercaptoethanol (all from ThermoFisher). *Fgf4*-mutant cell lines were cultured in 2i + LIF supplemented with 10% FBS. Cells were passaged every two to three days, and detached with trypsin (PAN Biotech) or Accutase (Sigma-Aldrich).

Cell lines

All cell lines generated in this study were derived from the E14tg2a wild-type line (Hooper et al., 1987). The GATA4-mCherry inducible line used for single cell RNA sequencing has been described previously (Raina et al., 2021). The *Spry4*$^{H2B\text{-}Venus/+}$-reporter line was generated with a previously described targeting construct (Morgani et al., 2018) using lipofectamine 2000 according manufacturer's instructions (Thermo Fisher Scientific). Correctly targeted clones were identified via long-range PCR as described in (Morgani et al., 2018). GATA6-mCherry inducible lines were established as described for GATA4-mCherry inducible lines in (Raina et al., 2021), but replacing the *Gata4* with a *Gata6* coding sequence in the PiggyBac vector for inducible gene expression. We established multiple clonal lines and tested them for GATA6-mCherry induction levels upon dox-treatment by flow cytometry. Three independent clones with induction levels similar or slightly higher than the previously established GATA4-mCherry inducible lines were selected for the experiment shown in Fig. 5D, and a single clonal line was chosen for all other experiments. Newly generated *Spry4*$^{H2B\text{-}Venus/+}$-reporter and GATA6-mCherry inducible cell lines were checked for karyotypic abnormalities. To label nuclei for time lapse imaging cells were transfected with pCX-H2B-Cerulean- IRES-puro (Schumacher et al., 2023). Cell lines carrying PiggyBac transgenes were kept under appropriate selection to prevent transgene repression over passaging.

652 ## sgRNA cloning and generation of single-gene mutants

653 For mutagenesis of individual genes via CRISPR/Cas9, gene targeting sgRNAs (Supp
654 Table 7) were cloned into pX459 (Addgene plasmid #48139) using BbsI (NEB) overhangs
655 following Ran et al., 2013 (Ran et al., 2013). Clonal mutant lines were generated using a
656 combination of sgRNAs with targeting sequences 100 to 200 bp apart in the genome. Single
657 sgRNAs were used when generating polyclonal lines. For validation experiments of the
658 CRISPR screen (Figs 1 and 2), we selected the most enriched sgRNA in sorted cells. A total
659 of 1 µg of sgRNA containing px459 vectors was mixed with a final concentration of 0.04 µg/ml
660 Lipofectamine 2000 (Thermo Fisher Scientific) in Opti-MEM (Gibco) according to the
661 manufacturer's protocol. For the generation of clonal lines, cells were seeded at clonal density
662 into 10 cm dishes after transfection, for polyclonal experiments approximately 50k cells/cm^2
663 were seeded. To enrich for successfully transfected cells, selection with 1.5 µg/ml puromycin
664 was started 24 h after transfection for 48 h. To establish clonal lines, single-cell derived
665 colonies were picked 4 to 6 d after transfection and expanded. For molecular characterization
666 of genetic lesions, genomic DNA was purified with Terra™ PCR Direct Genotyping Kit
667 (Takara), followed by PCR amplification and Sanger sequencing of specific genomic regions
668 encompassing the target site.
669

670 ## Genome-wide CRISPR Screen

671 To generate stably CAS9-expressing *Spry4*$^{H2B\text{-}Venus/+}$ reporter cells, cells were transduced with
672 lentiCas9-Blast lentiviral particles (Addgene #52962-LV) at a multiplicity of infection of
673 approximately 0.1. Transduction was performed with attached cells, 20 h after seeding at 20
674 000 cells/cm^2, in presence of 5 µg/ml Polybrene in ESL. Continuous blasticidin (15 µg/ml,
675 Gibco) selection was started 24 h after transduction. Lentiviral particles of the genome-wide
676 gRNA library Brie (Addgene #73633) were generated according to standard protocols (Doench
677 et al., 2016). For library transduction, 150 * 10^6 CAS9-expressing *Spry4*$^{H2B\text{-}Venus/+}$ reporter cells
678 were detached and mixed with the virus library in ESL with 5 µg/ml Polybrene. The following
679 day, the same number of cells was reseeded and put under selection with puromycin (1.5
680 µg/ml, Sigma-Aldrich). Comparing cell counts with and without selection indicated a
681 transduction efficiency of 25%, resulting in a >400-fold coverage of transduced cells per gRNA.
682 In all subsequent steps, at least 31 * 10^6 cells were processed to maintain gRNA coverage.
683 To identify gRNAs enriched in cell populations with high and low *Spry*4:H2B-Venus
684 expression, at least 0.5 * 10^6 cells with the lowest or highest 1% of *Spry*4:H2B-Venus
685 fluorescence, or 3 * 10^6 cells with the lowest or highest 5% of *Spry*4:H2B-Venus fluorescence
686 were FAC sorted and their DNA isolated by column-based genomic DNA purification (Monarch

687 Genomic DNA Purification Kit, NEB). For reference, the genomic DNA of 31 * 10^6 non-sorted
688 control cells was purified in parallel. The integrated gRNA was PCR amplified using Pfu
689 polymerase (prepared in house) with a sample specific, sequencing adapter and index
690 containing primers (Supp Table 7; Carlini et al., 2021) using the complete purified genomic
691 DNA as template. PCR-samples were purified with the SPRIselect reagent (Beckman Coulter)
692 with double-sided size selection. Briefly, 0.5x SPRIselect was added to each sample,
693 incubated for 5 min at RT and the SPRIselect removed with a magnet. This supernatant was
694 again mixed with 1.2x SPRIselect, incubated and then discarded. After washing the beads,
695 the DNA library was eluted from the beads and used for sequencing.
696 Paired-End Illumina Sequencing with a read length of 150 bp pairs was performed with at least
697 10 * 10^6 reads per sorted sample and 30 * 10^6 reads for the unsorted library controls. The raw
698 reads were trimmed using Cutadapt (Martin, 2011) to remove the vector binding sequence.
699 The reads were mapped to individual gRNAs, counted using *norm-method total* and
700 statistically tested on the targeted gene levels using *gene-lfc-method alphamean* with Mageck
701 (W. Li et al., 2014). Hits were selected based on the false discovery rate.
702

703 Immunostaining

704 Immunostaining was performed as previously described (Schröter et al., 2015), Briefly, cells
705 were washed with PBS containing Calcium and Magnesium, followed by fixation with 4%
706 paraformaldehyde (Histofix, Sigma-Aldrich) for 15 min. Cells were permeabilized and blocked
707 by rinsing and washing three times with PBS with 0.1% Triton X-100 and 1.0% bovine serum
708 albumin (PBT-BSA). Primary antibodies (Anti-mouse NANOG (Affymetrix eBioscience,
709 Cat.:14-5761), Anti-SOX17 (R&D systems, Cat.: AF1924)) were diluted 1:200 in PBT-BSA
710 and incubated with the cells overnight at 4 °C. The next day, cells were washed in PBT-BSA
711 and incubated with Alexa Fluor-conjugated secondary antibodies at 4 µg/ml (Invitrogen/Life
712 Technologies) and Hoechst 33342 at 1 µg/ml (Invitrogen) in PBT-BSA in the dark for 2 h.
713 Finally, samples were rinsed and washed with PBS and imaged in a mounting medium
714 consisting of 80% glycerol, 16% PBS and 4% n-propyl-gallate.
715

716 Immunoblotting

717 For western blot analysis of MED12 and ppERK, cells were washed twice with ice-cold PBS,
718 supplemented with 1 mM activated orthovanadate in case of ppERK detection. Cells were
719 mechanically detached in lysis buffer, based on commercially available lysis buffer (Cell
720 Signaling) supplemented with benzonase (Sigma-Aldrich), cOmplete EDTA-free protease
721 inhibitor cocktail (Roche), phosphate inhibitors P1 and P2 (Sigma). The lysates were snap

722 frozen in liquid nitrogen twice and centrifuged. Protein concentration in the supernatant was
723 measured with a micro BCA assay (Thermo Scientific). For western analysis, 20 µg of protein
724 per sample were denatured by adding 5x Laemelli buffer and incubation at 95 °C for 5 min.
725 The SDS-PAGE was run in 1x MOPS buffer (ThermoFisher) with 5 mM sodium-bisulfate and
726 immediately transferred onto methanol-activated PVDF membranes. Transfer was performed
727 in transfer buffer (12mM Tris-Base, 96mM Glycine, 20% methanol) at 40 V for 1.5 h in a
728 NuPage transfer system (ThermoFisher). Membranes were blocked at RT for 1 h in Intercept
729 blocking buffer (LI-COR), which was also used for the dilution and incubation with the primary
730 antibodies anti-Tubulin 1:10000 (T6074, Sigma), anti-pERK1/2 1:1000 (4370S, Cell
731 Signaling), anti-total ERK1/2 1:1000 (ab36991, Abcam) or anti-Med12 (1:250, A300-774A,
732 Bethyl Laboratories). Appropriate secondary antibodies (IRdyes, LI-COR) were used at a
733 dilution of 1:5000. Blots were imaged on an Odyssey CLx (LI-COR). Quantification of ppERK
734 bands was performed using the gel quantification tool in Fiji, using the combined intensities of
735 ERK1 and ERK2 bands, and normalizing ppERK by total ERK signals.
736

737 Imaging

738 Tilescans of immunostainings were imaged with a Leica SP8 confocal microscope (Leica
739 Microsystems) with a 63x 1.4 NA oil immersion objective. Images were analyzed in Fiji
740 (Schindelin et al., 2013). For segmentation, StarDist 2D (Schmidt et al., 2018) was used using
741 the versatile (fluorescent nuclei) model and default post processing parameters. Mean
742 fluorescence intensity was measured in segmented cells in all acquired channels. Cells with
743 a nuclear area smaller than 40 μm^2 were filtered out. To determine fluorescence intensity
744 threshold values for the classification of cell types, we manually selected thresholds that best
745 bisected the bimodal expression profiles of the lineage markers. The same thresholds were
746 applied to different samples in a single experiment.
747 Images of live *Spry4*$^{H2B\text{-}Venus/+}$-reporter cells were acquired with an Olympus IX81 widefield
748 microscope, equipped with a stage top incubator (ibidi), pE4000 illumination (CoolLED),
749 ORCA-Quest qCMOS camera (Hamamatsu) with a 63x 1.35 NA oil immersion objective.
750 Hardware was controlled by Olympus CellSens Software. Time lapse imaging was performed
751 with a 40x 0.9 NA objective on an Olympus IX81 widefield microscope, equipped with an LED-
752 based illumination system (pE4000, CoolLED) and an iXon 888 EM-CCD camera (Andor).
753 MicroManager (Edelstein et al., 2010) was used to control the hardware. Images were taken
754 every 10 min. Tracking was performed with the manual tracking function in Trackmate v7
755 (Ershov et al., 2022) and fluorescence intensity was measured as the mean intensity in a spot
756 with a 4 µm radius within the nucleus. In R, tracks were smoothed with a rolling average over

757 7 frames. For ROC analysis the R package pROC (Robin et al., 2011) was applied and the
758 optimal threshold was defined by the Youden's J statistic (Youden, 1950).
759

760 Flow cytometry

761 Analysis of *Spry4*:H2B-Venus reporter expression in live or fixed cells was performed on a
762 LSRII flow cytometer (BD Biosciences). Cell sorting and analysis of GATA6-mCherry
763 expression was carried out using a FACS Aria Fusion (BD Biosciences). Primary data analysis
764 including gating single cells based on SSC and FSC was done with FlowJo version 9 (BD
765 Biosciences).
766

767 Clonogenicity Assay

768 Clonogenicity assays were performed according to (Kalkan et al., 2017). Briefly, 1 * 10^4
769 cells/cm^2 were seeded in 2i + LIF for 24 h, followed by differentiation in N2B27 for 48 h. Control
770 wells for each parental cell line were kept in 2i + LIF. Cells were then detached with Accutase
771 to single cells, and 500 cells were reseeded into 6-well plates with 2i + LIF + 10% FBS. 10%
772 FBS were included to support survival of *Fgf4*-mutant cells.
773 After 5 d, the colonies formed were fixed and stained with an alkaline phosphatase assay kit
774 (Sigma-Aldrich) to distinguish pluripotent and differentiated colonies. Tile scans of the wells
775 were acquired with an Olympus IX81 widefield microscope with a 4x 0.16 NA objective. We
776 applied background subtraction, gaussian blurring, Otsu-thresholding, and conversion of
777 images to a binary mask in ImageJ, and then used the *AnalyzeParticles* function to set
778 thresholds for size and circularity and to determine the number of colonies. Colony numbers
779 were normalized to the number of colonies obtained in the control.
780

781 Bulk RNA sequencing

782 For bulk RNA sequencing, cells were seeded at a density between 3.5 and 5.5 * 10^4 cells/cm^2
783 in 2i or N2B27 + Chiron + LIF, followed by stimulation under indicated conditions. Replicates
784 were obtained either from independent biological experiments (Fig. 3 A, B) or from both
785 independent biological experiments and independent *Med12*-mutant lines (Fig. 3F, G). RNA
786 isolation was performed with TRIzol (ambion) according to the manufacturer's instructions.
787 Sequencing libraries were prepared on polyA-enriched RNAs, followed by paired-end
788 sequencing at a read-length of 150 bp and depth of approximately 30 * 10^6 reads per sample.
789 Strand-specific libraries were generated only for the FGF-titration experiment (Fig. 1 Supp 1)
790 and the differentiation of the *Med12* wild-type and mutant cells (Fig. 3A, B). Raw reads were

791 mapped to the mouse genome (GRCm39, release 108 (both *Med12* mutant experiments) or
792 release 97 (FGF titration experiment) with hisat2 (v2.1.0; Kim et al., 2019). SeqMonk was used
793 to quantify counts per gene, either as TPM or as raw counts as input for downstream DESeq2
794 analysis (Love et al., 2014) for identification of differentially expressed genes.
795 Differentiation delay in Med12 mutants was estimated according to (Lackner et al., 2021). We
796 first determined the expression change of the naïve marker genes *Nanog*, *Esrrb*, *Tbx3*,
797 *Tfcp2l1*, *Klf4*, *Prdm14* and *Zfp4* in *Med12*-mutant and wild-type cells, and then plotted the
798 Euclidean distance of this expression change to that of the time-resolved dataset from Lackner
799 et al., 2021.
800 Signaling footprint analysis in *Med12* mutants was performed similarly to Lacker et al., 2021.
801 This study defined a specific set of target genes for each pluripotency associated signaling
802 system based on gene expression changes in knockouts of signaling genes. A signaling
803 footprint for a knockout line can then be determined from the difference in the expression of
804 pathway footprint genes to the wild-type line after 24 h of differentiation. Measures for the
805 signaling footprint are the Spearman correlation between each knockout line and the
806 respective pathway defining knockout, and the ratio between the sum of expression fold
807 changes between a knockout line and the respective pathway defining knockout, defined as
808 pathway activity. To compare the *Med12* mutant data from this study, the wild type conditions
809 were used for batch correction.
810

811 # Cell multiplexing and scRNA sequencing

812 Cells for scRNAseq were seeded at a density of 3.5 * 10^4 cells/cm^2 in 6-well plates in 2i + LIF
813 and grown overnight. The next morning, induction in 2i + LIF + dox was first started in the
814 mutant clones, and 4 h later in the wild-type lines. After 8h and 4 h, respectively, induction was
815 stopped by washing once with N2B27, followed by 20 h of differentiation in N2B27. Controls
816 for each cell line were continuously kept in 2i + LIF. For sequencing, cells were washed three
817 times with PBS and detached with Accutase. Accutase was removed by centrifugation and 1
818 * 10^6 cells per sample were resuspended in PBS + 0.04 % BSA and immediately used for
819 multiplexing labeling following the protocol of 10x Genomics for samples with a viability above
820 80 % (Cell Multiplexing Oligo Labeling for Single Cell RNA Sequencing Protocols with Feature
821 Barcode technology, CG000391). Briefly, cells were spun down once again, resuspended with
822 individual cell multiplexing oligos (CMO no. 301 to 310) and incubated for 5 min at RT. Cells
823 were washed twice with PBS + 1 % BSA and passed through a cell strainer (FALCON, mesh
824 size 35 µm). A total of 1.2 * 10^5 single cells from all samples were pooled at equal ratios, and
825 4 * 10^4 were used for droplet generation, corresponding to a target number of 2.4 * 10^4 cell-
826 containing droplets. Droplet generation, lysis, mRNA and cell barcode capture, and generation

827 of both the gene expression library as well as the cell multiplexing library was performed
828 following the instructions by 10x genomics (Chromium Next GEM Single Cell 3' Reagent Kits
829 v3.1 (Dual Index) with Feature Barcode technology for Cell Multiplexing, CG000388).
830 Specifically, we chose 11 PCR cycles for cDNA amplification and 10 cycles for the sample
831 index PCR. Concentration and insert size distribution for both the gene expression library and
832 the cell multiplexing library were determined with a BioAnalyzer High Sensitivity DNA Assay
833 (Agilent). Sequencing was performed on a NovaSeq 6000 on multiple flowcells with a paired-
834 end 150 bp configuration. In total $1.2 * 10^9$ and $2.3 * 10^8$ read pairs were obtained for the gene
835 expression and multiplexing library, respectively.
836 Demultiplexing to the individual samples, based on the cell multiplexing barcode and
837 alignment to the mouse genome mm10 (GENCODE vM23/Ensembl 98, obtained from 10x
838 Genomics) was performed with CellRanger (version 7.1.0, 10x Genomics). Downstream
839 analysis was performed in R with Seurat v5 (Hao et al., 2023). We first filtered cells by
840 removing barcodes with ≤ 2500 detected genes and ≥15 % of reads aligned to mitochondrial
841 genes, retaining between 1100 and 1700 cells per sample with median mRNA counts per cell
842 between 23233 and 27890 in the different samples. mRNA counts for each gene were
843 normalized by dividing its counts by the total number of counts per cell, multiplied by 10000.
844 Log1p transformation was applied before plotting expression data as violin plots. For
845 downstream analysis and representation of gene expression as heatmaps, centering counts
846 for each feature and scaling to its standard deviation was applied. Principal component
847 analysis was performed on the 2000 most variable features in the relevant subset of cells. The
848 resolution of the Louvain clustering algorithm was set to 0.05 when clustering multiple
849 samples. In case of Jaccard-Index estimation the clustering resolution was set to 0.15 and the
850 clustering was performed on each sample separately. 100-fold repetition of this clustering
851 approach with a random subset of the data with 70 % of the cells allowed the calculation of a
852 Jaccard-index, as previously described (Tang et al., 2021). For annotation of the Epi- and PrE-
853 fate, the cells of the differentiated samples were integrated with Seurat integration based on
854 the *rpca* reduction. Differentially expressed genes between cell states and genotypes were
855 identified with the *FindMarkers* function in Seurat with a minimal expression difference in the
856 log1p transformed expression values of 0.5. Biological noise was quantitated and
857 distinguished from modeled technical noise in local neighborhoods of each cell with VarID2
858 (Rosales-Alvarez et al., 2023).
859

Data and code availability

Sequencing data from this paper has been deposited at GEO with accession number GSE253609. All code used for analysis and visualization, together with a list of the R packages used, is available from the authors upon request.

Bibliography

Apostolou, E., Ferrari, F., Walsh, R. M., Bar-Nur, O., Stadtfeld, M., Cheloufi, S., Stuart, H. T., Polo, J. M., Ohsumi, T. K., Borowsky, M. L., Kharchenko, P. V., Park, P. J., & Hochedlinger, K. (2013). Genome-wide chromatin interactions of the nanog locus in pluripotency, differentiation, and reprogramming. *Cell Stem Cell*, *12*(6), 699–712. https://doi.org/10.1016/j.stem.2013.04.013

Aranda-Orgilles, B., Saldaña-Meyer, R., Wang, E., Trompouki, E., Fassl, A., Lau, S., Mullenders, J., Rocha, P. P., Raviram, R., Guillamot, M., Sánchez-Díaz, M., Wang, K., Kayembe, C., Zhang, N., Amoasii, L., Choudhuri, A., Skok, J. A., Schober, M., Reinberg, D., … Aifantis, I. (2016). MED12 Regulates HSC-Specific Enhancers Independently of Mediator Kinase Activity to Control Hematopoiesis. *Cell Stem Cell*, *19*(6), 784–799. https://doi.org/10.1016/j.stem.2016.08.004

Athanasouli, P., Balli, M., De Jaime-Soguero, A., Boel, A., Papanikolaou, S., van der Veer, B. K., Janiszewski, A., Vanhessche, T., Francis, A., El Laithy, Y., Nigro, A. Lo, Aulicino, F., Koh, K. P., Pasque, V., Cosma, M. P., Verfaillie, C., Zwijsen, A., Heindryckx, B., Nikolaou, C., & Lluis, F. (2023). The Wnt/TCF7L1 transcriptional repressor axis drives primitive endoderm formation by antagonizing naive and formative pluripotency. *Nature Communications*, *14*(1), 1–19. https://doi.org/10.1038/s41467-023-36914-1

Betschinger, J., Nichols, J., Dietmann, S., Corrin, P. D., Paddison, P. J., & Smith, A. (2013). Exit from pluripotency is gated by intracellular redistribution of the bHLH transcription factor Tfe3. *Cell*, *153*(2), 335–347. https://doi.org/10.1016/j.cell.2013.03.012

Carlini, V., Gretarsson, K. H., & Hackett, J. A. (2021). Genome-scale CRISPR screening for regulators of cell fate transitions. In *Methods in Molecular Biology* (Vol. 2214, pp. 91–108). Humana Press Inc. https://doi.org/10.1007/978-1-0716-0958-3_7

Chazaud, C., & Yamanaka, Y. (2016). Lineage specification in the mouse preimplantation embryo. *Development (Cambridge)*, *143*(7), 1063–1074. https://doi.org/10.1242/DEV.128314

Doench, J. G., Fusi, N., Sullender, M., Hegde, M., Vaimberg, E. W., Donovan, K. F., Smith, I., Tothova, Z., Wilen, C., Orchard, R., Virgin, H. W., Listgarten, J., & Root, D. E. (2016). Optimized sgRNA design to maximize activity and minimize off-target effects of CRISPR-Cas9. *Nature Biotechnology*, *34*(2), 184–191. https://doi.org/10.1038/nbt.3437

Donner, A. J., Ebmeier, C. C., Taatjes, D. J., & Espinosa, J. M. (2010). CDK8 is a positive regulator of transcriptional elongation within the serum response network. *Nature Structural and Molecular Biology*, *17*(2), 194–201. https://doi.org/10.1038/nsmb.1752

Edelstein, A., Amodaj, N., Hoover, K., Vale, R., & Stuurman, N. (2010). Computer control of microscopes using μManager. *Current Protocols in Molecular Biology*, *Chapter 14*(SUPPL. 92). https://doi.org/10.1002/0471142727.MB1420S92

Ershov, D., Phan, M. S., Pylvänäinen, J. W., Rigaud, S. U., Le Blanc, L., Charles-Orszag, A., Conway, J. R. W., Laine, R. F., Roy, N. H., Bonazzi, D., Duménil, G., Jacquemet, G., & Tinevez, J. Y. (2022). TrackMate 7: integrating state-of-the-art segmentation algorithms into tracking pipelines. *Nature Methods*, *19*(7), 829–832. https://doi.org/10.1038/s41592-022-01507-1

Fawcett, T. (2006). An introduction to ROC analysis. *Pattern Recognition Letters*, *27*(8), 861–874. https://doi.org/10.1016/J.PATREC.2005.10.010

Fujikura, J., Yamato, E., Yonemura, S., Hosoda, K., Masui, S., Nakao, K., Miyazaki, J. I., & Niwa, H. (2002). Differentiation of embryonic stem cells is induced by GATA factors. *Genes & Development*, *16*(7), 784–789. https://doi.org/10.1101/GAD.968802

Hanna, R. E., & Doench, J. G. (2020). Design and analysis of CRISPR–Cas experiments. In *Nature Biotechnology* (Vol. 38, Issue 7, pp. 813–823). Nature Research. https://doi.org/10.1038/s41587-020-0490-7

Hao, Y., Stuart, T., Kowalski, M. H., Choudhary, S., Hoffman, P., Hartman, A., Srivastava, A., Molla, G., Madad, S., Fernandez-Granda, C., & Satija, R. (2023). Dictionary learning for integrative, multimodal and scalable single-cell analysis. *Nature Biotechnology*, 1–12. https://doi.org/10.1038/s41587-023-01767-y

Hooper, M., Hardy, K., Handyside, A., Hunter, S., & Monk, M. (1987). HPRT-deficient (Lesch-Nyhan) mouse embryos derived from germline colonization by cultured cells. *Nature*, *326*(6110), 292–295. https://doi.org/10.1038/326292A0

Kagey, M. H., Newman, J. J., Bilodeau, S., Zhan, Y., Orlando, D. A., Van Berkum, N. L., Ebmeier, C. C., Goossens, J., Rahl, P. B., Levine, S. S., Taatjes, D. J., Dekker, J., & Young, R. A. (2010). Mediator and cohesin connect gene expression and chromatin architecture. *Nature*, *467*(7314), 430–435. https://doi.org/10.1038/nature09380

Kalkan, T., Bornelöv, S., Mulas, C., Diamanti, E., Lohoff, T., Ralser, M., Middelkamp, S., Lombard, P., Nichols, J., & Smith, A. (2019). Complementary Activity of ETV5, RBPJ, and TCF3 Drives Formative Transition from Naive Pluripotency. *Cell Stem Cell*, *24*(5), 785-801.e7. https://doi.org/10.1016/j.stem.2019.03.017

Kalkan, T., Olova, N., Roode, M., Mulas, C., Lee, H. J., Nett, I., Marks, H., Walker, R., Stunnenberg, H. G., Lilley, K. S., Nichols, J., Reik, W., Bertone, P., & Smith, A. (2017). Tracking the embryonic stem cell transition from ground state pluripotency. *Development (Cambridge)*, *144*(7), 1221–1234. https://doi.org/10.1242/dev.142711

Kalkan, T., & Smith, A. (2014). Mapping the route from naive pluripotency to lineage specification. *Philosophical Transactions of the Royal Society B: Biological Sciences*, *369*(1657). https://doi.org/10.1098/RSTB.2013.0540

Kang, M., Piliszek, A., Artus, J., & Hadjantonakis, A. K. (2013). FGF4 is required for lineage restriction and salt-and-pepper distribution of primitive endoderm factors but not their initial expression in the mouse. *Development (Cambridge)*, *140*(2), 267–279. https://doi.org/10.1242/DEV.084996

Kim, D., Paggi, J. M., Park, C., Bennett, C., & Salzberg, S. L. (2019). Graph-based genome alignment and genotyping with HISAT2 and HISAT-genotype. *Nature Biotechnology*, *37*(8), 907–915. https://doi.org/10.1038/S41587-019-0201-4

Knuesel, M. T., Meyer, K. D., Donner, A. J., Espinosa, J. M., & Taatjes, D. J. (2009). The human CDK8 subcomplex is a histone kinase that requires Med12 for activity and can function independently of mediator. *Molecular and Cellular Biology*, *29*(3), 650–661. https://doi.org/10.1128/MCB.00993-08

Lackner, A., Sehlke, R., Garmhausen, M., Giuseppe Stirparo, G., Huth, M., Titz-Teixeira, F., Lelij, P., Ramesmayer, J., Thomas, H. F., Ralser, M., Santini, L., Galimberti, E., Sarov, M., Stewart, A. F., Smith, A., Beyer, A., & Leeb, M. (2021). Cooperative genetic networks drive embryonic stem cell transition from naïve to formative pluripotency. *The EMBO Journal*, *40*(8). https://doi.org/10.15252/embj.2020105776

Li, M., Yu, J. S. L., Tilgner, K., Ong, S. H., Koike-Yusa, H., & Yusa, K. (2018). Genome-wide CRISPR-KO Screen Uncovers mTORC1-Mediated Gsk3 Regulation in Naive Pluripotency Maintenance and Dissolution. *Cell Reports*, *24*(2), 489–502. https://doi.org/10.1016/j.celrep.2018.06.027

Li, W., Xu, H., Xiao, T., Cong, L., Love, M. I., Zhang, F., Irizarry, R. A., Liu, J. S., Brown, M., & Liu, X. S. (2014). MAGeCK enables robust identification of essential genes from genome-scale CRISPR/Cas9 knockout screens. *Genome Biology*, *15*(12), 554. https://doi.org/10.1186/s13059-014-0554-4

Love, M. I., Huber, W., & Anders, S. (2014). Moderated estimation of fold change and dispersion for RNA-seq data with DESeq2. *Genome Biology*, *15*(12), 1–21. https://doi.org/10.1186/s13059-014-0550-8

Luyties, O., & Taatjes, D. J. (2022). The Mediator kinase module: an interface between cell signaling and transcription. *Trends in Biochemical Sciences*, *47*(4), 314–327. https://doi.org/10.1016/j.tibs.2022.01.002

Lynch, C. J., Bernad, R., Martínez-Val, A., Shahbazi, M. N., Nóbrega-Pereira, S., Calvo, I., Blanco-Aparicio, C., Tarantino, C., Garreta, E., Richart-Ginés, L., Alcazar, N., Graña-Castro, O., Gómez-Lopez, G., Aksoy, I., Muñoz-Martín, M., Martinez, S., Ortega, S., Prieto, S., Simboeck, E., … Serrano, M. (2020). Global hyperactivation of enhancers stabilizes human and mouse naive pluripotency through inhibition of CDK8/19 Mediator kinases. *Nature Cell Biology*, *22*(10), 1223–1238. https://doi.org/10.1038/s41556-020-0573-1

Martin, M. (2011). Cutadapt removes adapter sequences from high-throughput sequencing reads. *EMBnet.Journal*, *17*(1), 10–12. https://doi.org/10.14806/EJ.17.1.200

Morgani, S. M., & Brickman, J. M. (2015). LIF supports primitive endoderm expansion during pre-implantation development. *Development (Cambridge)*, *142*(20), 3488–3499. https://doi.org/10.1242/DEV.125021

Morgani, S. M., Saiz, N., Garg, V., Raina, D., Simon, C. S., Kang, M., Arias, A. M., Nichols, J., Schröter, C., & Hadjantonakis, A. K. (2018). A Sprouty4 reporter to monitor FGF/ERK signaling activity in ESCs and mice. *Developmental Biology*, *441*(1), 104–126. https://doi.org/10.1016/j.ydbio.2018.06.017

Neagu, A., van Genderen, E., Escudero, I., Verwegen, L., Kurek, D., Lehmann, J., Stel, J., Dirks, R. A. M., van Mierlo, G., Maas, A., Eleveld, C., Ge, Y., den Dekker, A. T., Brouwer, R. W. W., van IJcken, W. F. J., Modic, M., Drukker, M., Jansen, J. H., Rivron, N. C., … ten Berge, D. (2020). In vitro capture and characterization of embryonic rosette-stage pluripotency between naive and primed states. *Nature Cell Biology*, *22*(5), 534–545. https://doi.org/10.1038/S41556-020-0508-X

Nichols, J., Silva, J., Roode, M., & Smith, A. (2009). Suppression of Erk signalling promotes ground state pluripotency in the mouse embryo. *Development (Cambridge)*, *136*(19), 3215–3222. https://doi.org/10.1242/dev.038893

Nichols, J., & Smith, A. (2009). Naive and Primed Pluripotent States. In *Cell Stem Cell* (Vol. 4, Issue 6, pp. 487–492). https://doi.org/10.1016/j.stem.2009.05.015

Ornitz, D. M., & Itoh, N. (2015). The fibroblast growth factor signaling pathway. *Wiley Interdisciplinary Reviews: Developmental Biology*, *4*(3), 215–266. https://doi.org/10.1002/wdev.176

Park, M. J., Shen, H., Spaeth, J. M., Tolvanen, J. H., Failor, C., Knudtson, J. F., McLaughlin, J., Halder, S. K., Yang, Q., Bulun, S. E., Al-Hendy, A., Schenken, R. S., Aaltonen, L. A., & Boyer, T. G. (2018). Oncogenic exon 2 mutations in Mediator subunit MED12 disrupt allosteric activation of cyclin C-CDK8/19. *The Journal of Biological Chemistry*, *293*(13), 4870–4882. https://doi.org/10.1074/JBC.RA118.001725

Raina, D., Bahadori, A., Stanoev, A., Protzek, M., Koseska, A., & Schröter, C. (2021). Cell-cell communication through FGF4 generates and maintains robust proportions of

differentiated cell types in embryonic stem cells. *Development (Cambridge)*, *148*(21). https://doi.org/10.1242/DEV.199926

Ran, F. A., Hsu, P. D., Wright, J., Agarwala, V., Scott, D. A., & Zhang, F. (2013). Genome engineering using the CRISPR-Cas9 system. *Nature Protocols*, *8*(11), 2281–2308. https://doi.org/10.1038/NPROT.2013.143

Robin, X., Turck, N., Hainard, A., Tiberti, N., Lisacek, F., Sanchez, J. C., & Müller, M. (2011). pROC: An open-source package for R and S+ to analyze and compare ROC curves. *BMC Bioinformatics*, *12*(1), 1–8. https://doi.org/https://doi.org/10.1186/1471-2105-12-77

Rocha, P. P., Scholze, M., Bleiß, W., & Schrewe, H. (2010). Med12 is essential for early mouse development and for canonical Wnt and Wnt/PCP signaling. *Development (Cambridge)*, *137*(16), 2723–2731. https://doi.org/10.1242/dev.053660

Rosales-Alvarez, R. E., Rettkowski, J., Herman, J. S., Dumbović, G., Cabezas-Wallscheid, N., & Grün, D. (2023). VarID2 quantifies gene expression noise dynamics and unveils functional heterogeneity of ageing hematopoietic stem cells. *Genome Biology*, *24*(1). https://doi.org/10.1186/s13059-023-02974-1

Schindelin, J., Arganda-carreras, I., Frise, E., Kaynig, V., Pietzsch, T., Preibisch, S., Rueden, C., Saalfeld, S., Schmid, B., Tinevez, J., White, D. J., Hartenstein, V., Tomancak, P., & Cardona, A. (2013). Fiji - an Open Source platform for biological image analysis. *Nature Methods*, *9*(7). https://doi.org/10.1038/nmeth.2019.Fiji

Schmidt, U., Weigert, M., Broaddus, C., & Myers, G. (2018). Cell detection with star-convex polygons. *Lecture Notes in Computer Science*, *11071 LNCS*, 265–273. https://doi.org/https://doi.org/10.1007/978-3-030-00934-2_30

Schröter, C., Rué, P., Mackenzie, J. P., & Arias, A. M. (2015). FGF/MAPK signaling sets the switching threshold of a bistable circuit controlling cell fate decisions in embryonic stem cells. *Development (Cambridge)*, *142*(24), 4205–4216. https://doi.org/10.1242/DEV.127530/-/DC1

Schumacher, S., Fernkorn, M., Marten, M., Kim, Y. S., Bedzhov, I., & Schröter, C. (2023). Tissue-intrinsic Wnt signals antagonize Nodal-driven AVE differentiation. *BioRxiv*, 2023.05.19.541432. https://doi.org/10.1101/2023.05.19.541432

Smith, A. (2017). Formative pluripotency: The executive phase in a developmental continuum. *Development (Cambridge)*, *144*(3), 365–373. https://doi.org/10.1242/dev.142679

Soutourina, J. (2018). Transcription regulation by the Mediator complex. In *Nature Reviews Molecular Cell Biology* (Vol. 19, Issue 4, pp. 262–274). Nature Publishing Group. https://doi.org/10.1038/nrm.2017.115

Stevens, J. L., Cantin, G. T., Wang, G., Shevchenko, A., Shevchenko, A., & Berk, A. J. (2002). Transcription control by E1A and MAP kinase pathway via Sur2 mediator subunit. *Science*, *296*(5568), 755–758. https://doi.org/10.1126/SCIENCE.1068943

Szklarczyk, D., Franceschini, A., Wyder, S., Forslund, K., Heller, D., Huerta-Cepas, J., Simonovic, M., Roth, A., Santos, A., Tsafou, K. P., Kuhn, M., Bork, P., Jensen, L. J., & Von Mering, C. (2015). STRING v10: protein-protein interaction networks, integrated over the tree of life. *Nucleic Acids Research*, *43*(Database issue), D447–D452. https://doi.org/10.1093/NAR/GKU1003

Tang, M., Kaymaz, Y., Logeman, B. L., Eichhorn, S., Liang, Z. S., Dulac, C., & Sackton, T. B. (2021). Evaluating single-cell cluster stability using the Jaccard similarity index. *Bioinformatics*, *37*(15), 2212–2214. https://doi.org/10.1093/BIOINFORMATICS/BTAA956

1049 Tee, W. W., Shen, S. S., Oksuz, O., Narendra, V., & Reinberg, D. (2014). Erk1/2 activity
1050 promotes chromatin features and RNAPII phosphorylation at developmental promoters
1051 in mouse ESCs. *Cell*, *156*(4), 678–690. https://doi.org/10.1016/j.cell.2014.01.009
1052 Tutter, A. V., Kowalski, M. P., Baltus, G. A., Iourgenko, V., Labow, M., Li., E., & Kadam, S.
1053 (2009). Role for Med12 in regulation of Nanog and Nanog target genes. *Journal of*
1054 *Biological Chemistry*, *284*(6), 3709–3718. https://doi.org/10.1074/jbc.M805677200
1055 Villegas, F., Lehalle, D., Mayer, D., Rittirsch, M., Stadler, M. B., Zinner, M., Olivieri, D., Vabres,
1056 P., Duplomb-Jego, L., De Bont, E. S. J. M., Duffourd, Y., Duijkers, F., Avila, M.,
1057 Geneviève, D., Houcinat, N., Jouan, T., Kuentz, P., Lichtenbelt, K. D., Thauvin-Robinet,
1058 C., … Betschinger, J. (2019). Lysosomal Signaling Licenses Embryonic Stem Cell
1059 Differentiation via Inactivation of Tfe3. *Cell Stem Cell*, *24*(2), 257-270.e8.
1060 https://doi.org/10.1016/J.STEM.2018.11.021
1061 Wamaitha, S. E., del Valle, I., Cho, L. T. Y., Wei, Y., Fogarty, N. M. E., Blakeley, P., Sherwood,
1062 R. I., Ji, H., & Niakan, K. K. (2015). Gata6 potently initiates reprograming of pluripotent
1063 and differentiated cells to extraembryonic endoderm stem cells. *Genes & Development*,
1064 *29*(12), 1239–1255. https://doi.org/10.1101/GAD.257071.114
1065 Ying, Q. L., Wray, J., Nichols, J., Batlle-Morera, L., Doble, B., Woodgett, J., Cohen, P., &
1066 Smith, A. (2008). The ground state of embryonic stem cell self-renewal. *Nature*,
1067 *453*(7194), 519–523. https://doi.org/10.1038/nature06968
1068 Youden, W. J. (1950). INDEX FOR RATING DIAGNOSTIC TESTS. *Cancer*, *3*(1), 32–35.
1069 https://doi.org/10.1002/1097-0142(1950)3:1<32::AID-CNCR2820030106>3.0.CO;2-3

1070

1071

1072

Supplementary Figures

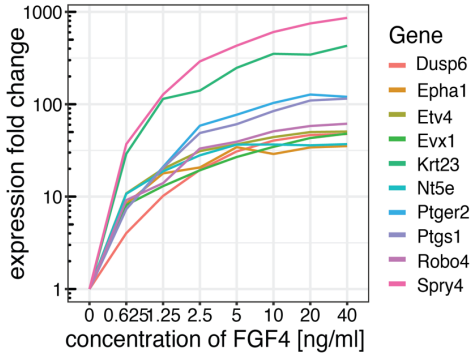

Fig. 1 Supp 1: *Spry4* is strongly upregulated upon FGF stimulation.
Expression fold change of the ten most upregulated genes upon FGF4 titration in *Fgf4* mutants. *Fgf4*-mutant *Spry4*$^{H2B\text{-}Venus/+}$ cells were transitioned from 2i + LIF medium containing 10% FBS to N2B27 supplemented with Chiron and LIF for 18 h, followed by 6 h of stimulation with indicated concentrations of FGF4 in N2B27 with Chiron.

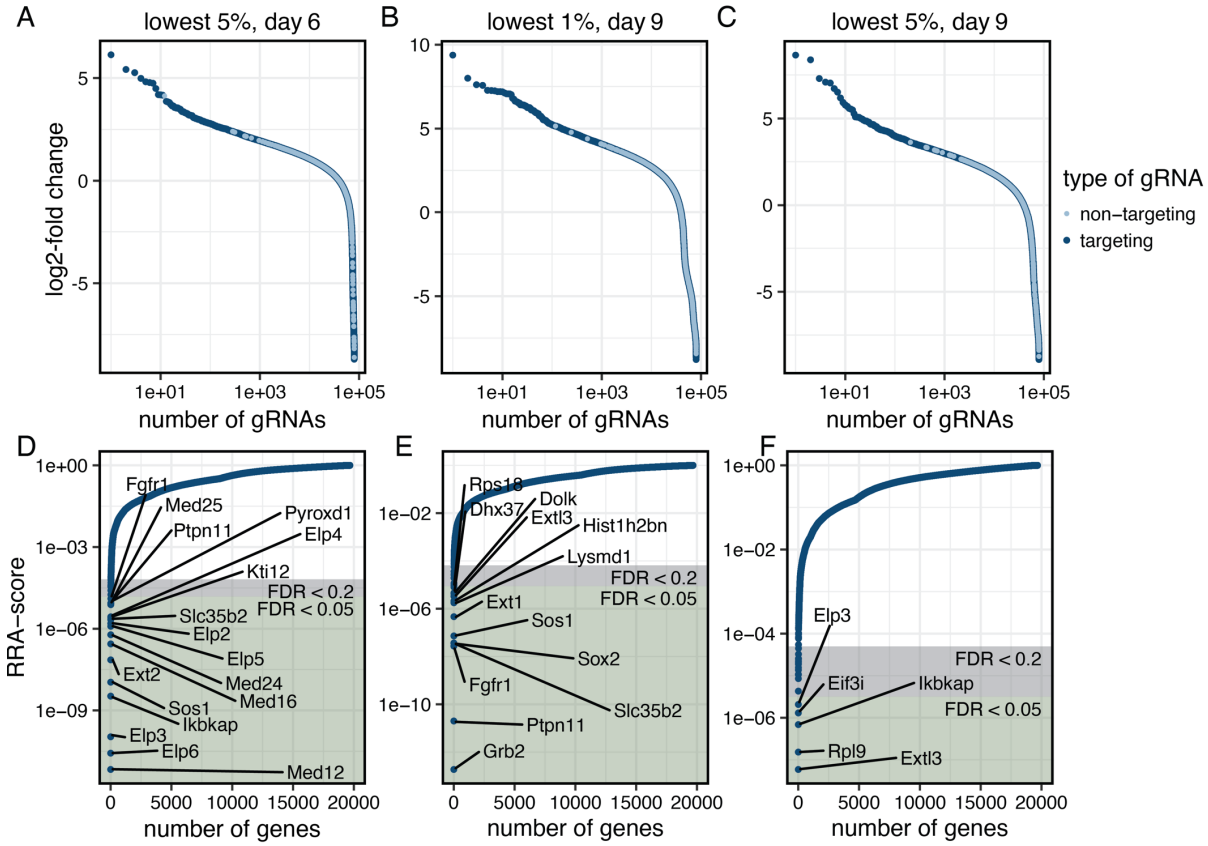

Fig. 1 Supp 2: Genome-wide CRISPR knockout screen results in robust enrichment of gRNAs and corresponding genes.
A - C Log 2-fold enrichment of gene-targeting (dark blue) and control gRNAs (light blue) in cells sorted for the lowermost 5% of H2B-Venus signal on day 6 after gRNA transduction (A), sorted for the

lowermost 1% on day 9 after transduction (B), or sorted for the the lowermost 5% on day 9 after transduction (C). **D** - **F** RRA scores for genes corresponding to enriched gRNAs identified in A - C.

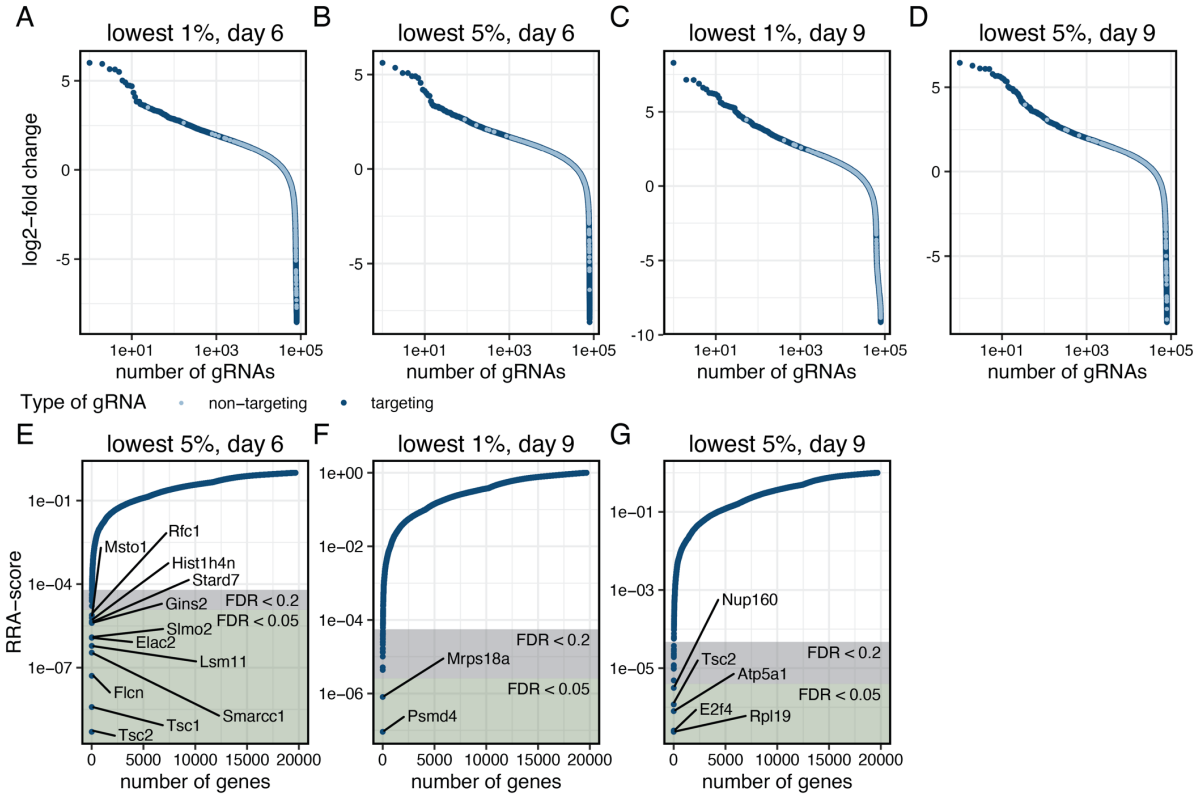

Fig. 2 Supp 1: Robust enrichment of gRNAs and corresponding genes that negatively regulate Spry4:H2B-Venus expression.

A - **D** Log 2-fold enrichment of gene-targeting (dark blue) and control gRNAs (light blue) in cells sorted for high H2B-Venus expression on different days as indicated.

E - **G** RRA scores for genes corresponding to enriched gRNAs identified in B - D. RRA scores for genes corresponding to gRNAs enriched in the 1% of the cells with highest fluorescence after 6 days are shown in Fig. 2A.

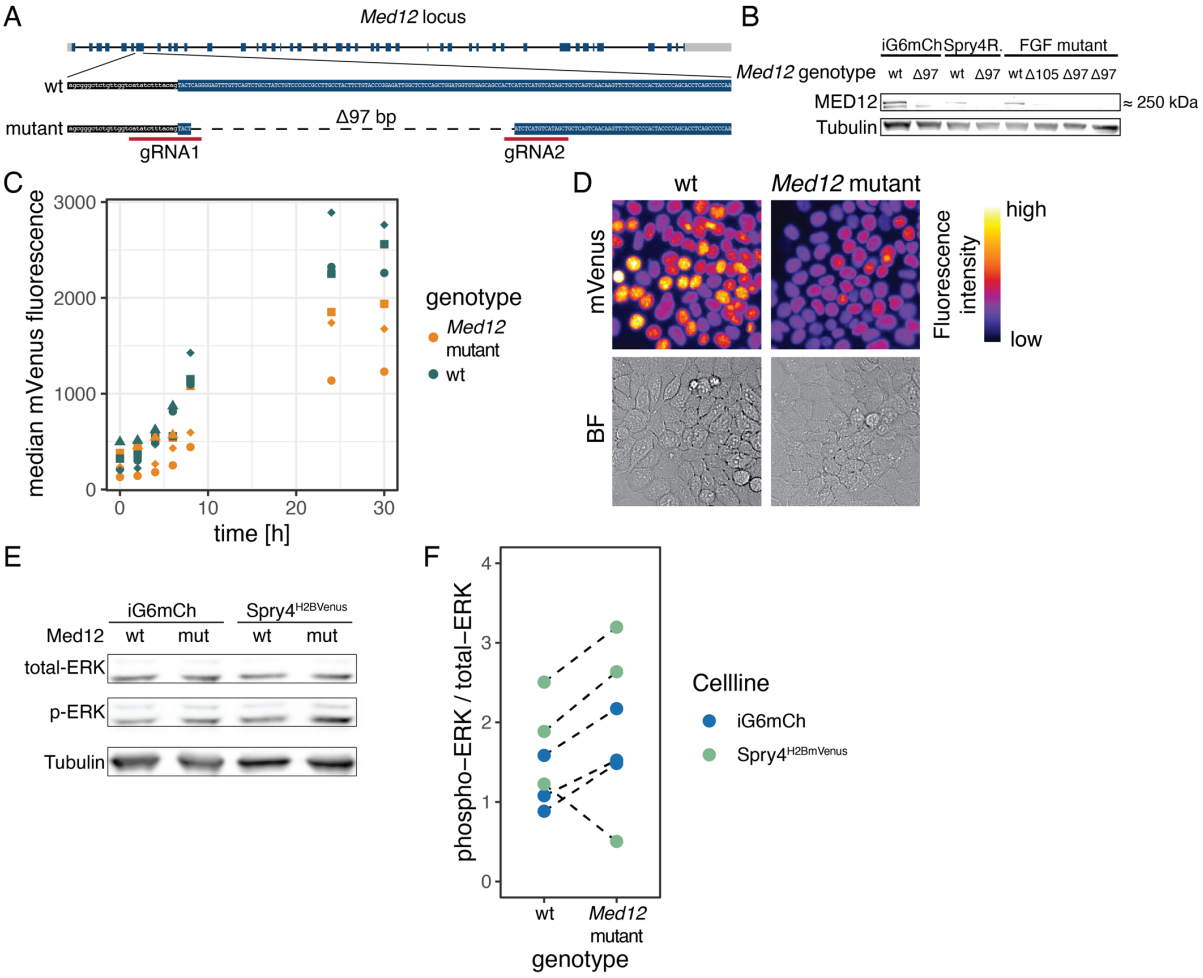

Fig. 3 Supp1: Generation of *Med12* mutant cell lines.

A Schematic of the *Med12* gene locus and the gRNAs used to create a *Med12* loss-of-function by deleting part of exon7.

B Immunoblotting of cell lysates from several monoclonal *Med12* mutant lines generated in different genetic genetic backgrounds, stained for MED12 and Tubulin.

C *Spry4*$^{H2B\text{-}Venus/+}$ Expression upon release from 2i + LIF to N2B27 in wild-type and *Med12*-mutant cells measured by flow cytometry. Data points show median fluorescence in each experiment. N = 3.

D H2B-Venus expression in live wild-type and *Med12*-mutant *Spry4*$^{H2B\text{-}Venus/+}$ cells after 24 h of growth in N2B27 following release from 2i + LIF.

E Immunoblotting of cell lysates from *Med12* wild type and *Med12*-mutant *Spry4*$^{H2B\text{-}Venus/+}$ and iGata6 mESCs, stained for Tubulin, total- and phopsho-ERK.

F Quantification of phospho-ERK signals from immunoblots, normalized to total-ERK. N=3.

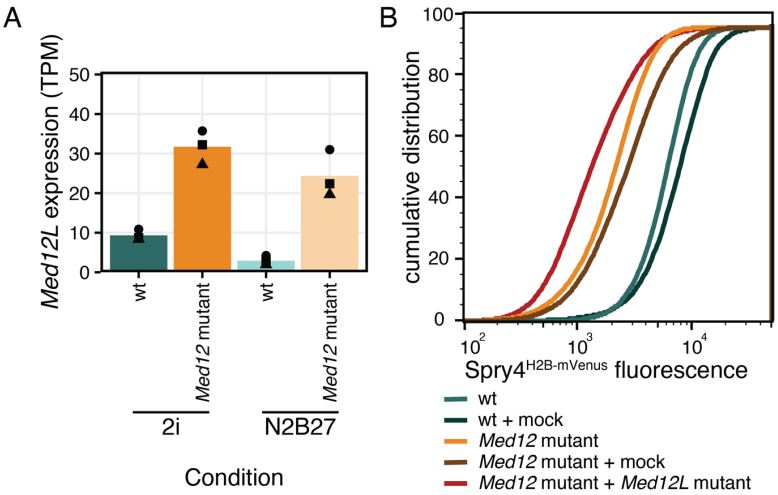

Fig. 3 Supp 2: *Med12l* is upregulated upon loss of *Med12*.

A Expression of *Med12l* in wild-type and *Med12*-mutant cells (data from RNA-seq experiment in Fig. 3A).

B H2B-Venus expression in untransfected wild-type and *Med12*-mutant cells, and after transfection with mock or *Med12l*-targeting gRNAs. Expression was measured by flow cytometry 7 d after transfection and culture in ES + LIF medium.

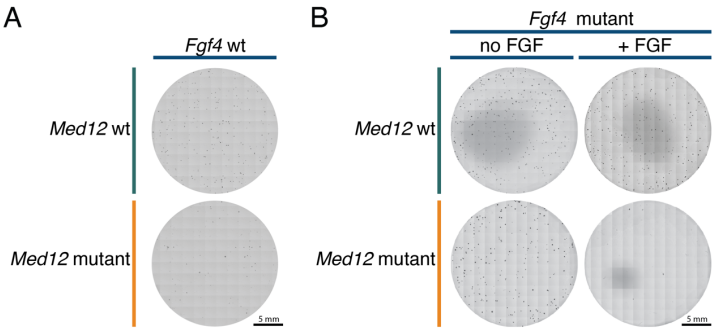

Fig. 4 Supp 1: Reduced clonogenicity in *Med12* mutants compared to wild type.

A and **B** Representative images of plates from the clonogenicity assay depicted in Fig. 4A, corresponding to quantifications shown in Fig. 4B. **A** shows plates with wild-type and *Med12*-mutant cells in an *Fgf4* wild type background, **B** shows plates with wild-type and *Med12*-mutant cells in an *Fgf4*-mutant background without (left) and with (right) FGF4 supplementation.

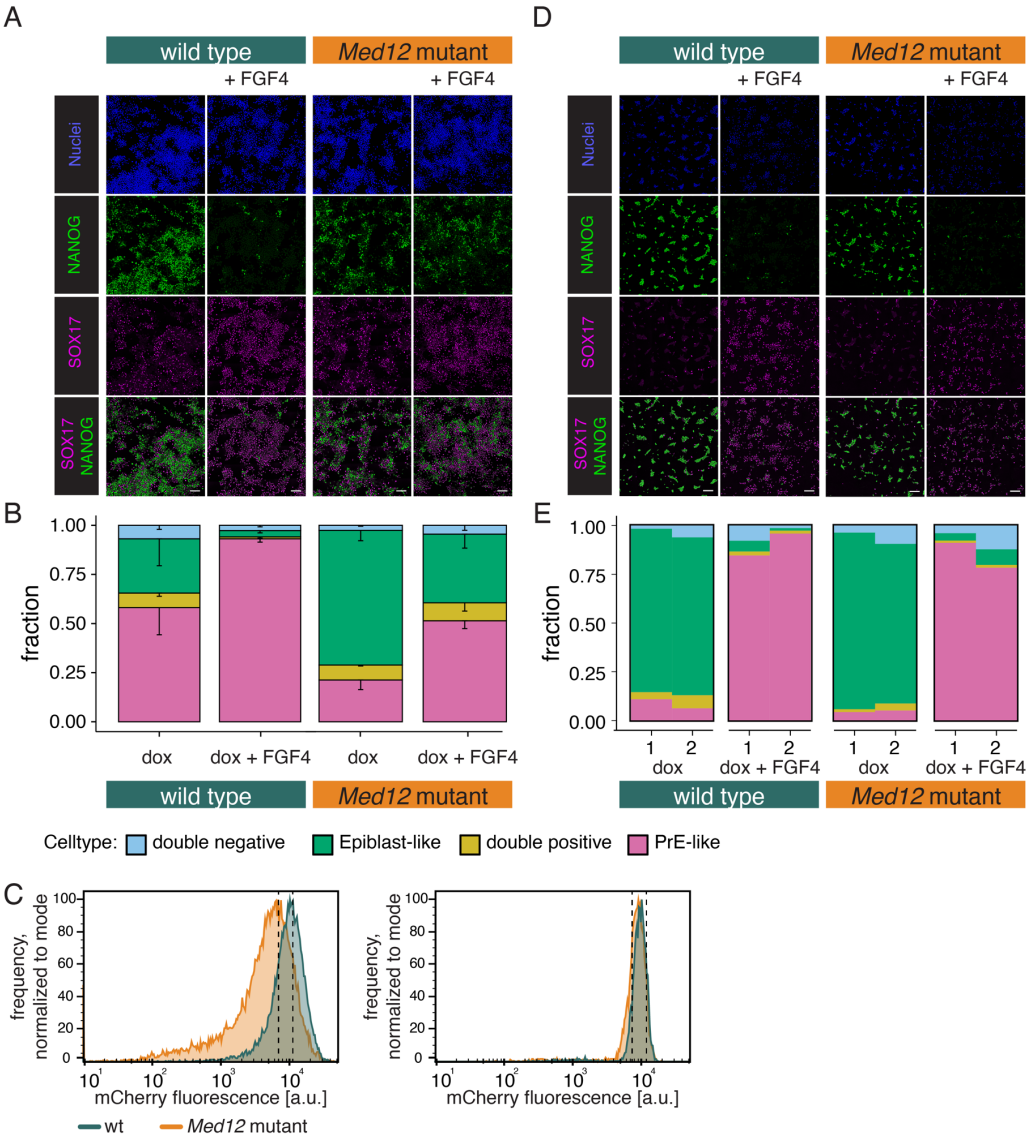

Fig. 5 Supp 1: Lower GATA6-mCherry induction levels limit PrE differentiation in *Med12* mutant cells.

A Immunostaining of the Epi-marker NANOG (green) and the PrE marker SOX17 (magenta) after 8 h of GATA6 induction and 20 h of differentiation with and without exogenous FGF4 in wild-type and *Med12*-mutant cells. Scale bar: 100 µm.

B Quantification of cell type proportions after differentiating wild-type and *Med12*-mutant cells as in (A). N=3, n > 1100 cells per replicate, error bars indicate SEM.

C Gata-mCherry fluorescence after 8 h of dox induction. Left shows distribution of expression levels in the whole population, right shows expression levels after flow sorting of cells with similar fluorescence intensity. Dashed lines indicate sorting gate.

D Immunostaining of the Epi-marker NANOG (green) and the PrE marker SOX17 (magenta) after 8 h of GATA6 induction, flow sorting as described in (C), reseeding and 20 h of differentiation with and without exogenous FGF4 in wild-type and *Med12*-mutant cells. Scale bar: 100 µm.

E Quantification of cell type proportions after differentiating wild-type and *Med12*-mutant cells as in (D). N=2, n > 500 cells per replicate.

1140

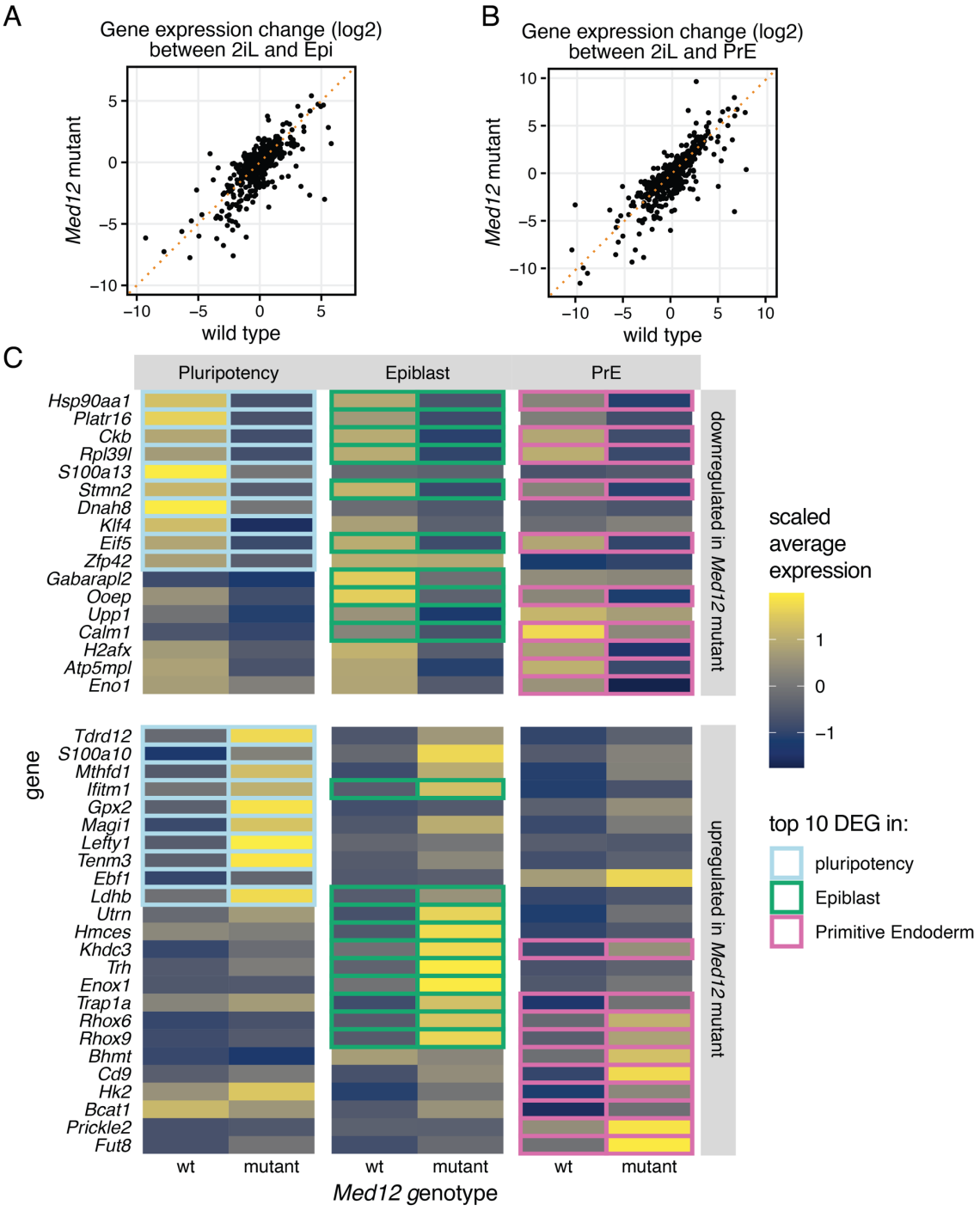

1141

1142 **Fig. 6 Supp 1:**

1143 **A** and **B** Expression change of each gene upon differentiation from pluripotency (2iL) to Epi (A) and
1144 PrE (B) in wild-type versus *Med12*-mutant cells. Dotted, orange line indicates the unity line.
1145 **C** Differentially expressed genes between *Med12* wild type and mutant cells for the three different cell
1146 states. Tile color shows scaled average gene expression, colored boxes indicate the 10 genes with the
1147 largest fold-change between *Med12* wild type and mutant cells in each cell state.

1148 # Supplementary Table legends

1149 **Supp Table 1**: Raw and processed data from CRISPR screen including detected counts of
1150 gRNAs and enriched genes.
1151
1152 **Supp Table 2**: Differentially expressed genes comparing wild-type and *Med12*-mutant cells in
1153 2i and after 24 h differentiation in N2B27.
1154
1155 **Supp Table 3**: Differentially expressed genes in *Fgf4*-mutant and *Fgf4 Med12* double mutant
1156 cells upon FGF4 stimulation in N2B27.
1157
1158 **Supp Table 4**: Raw and normalized counts of colonies detected in the colony formation assay.
1159
1160 **Supp Table 5**: Differentially expressed genes between the Epi- (cluster 1) and PrE-cells
1161 (cluster 0) determined by single cell RNA sequencing experiment.
1162
1163 **Supp Table 6**: Differentially expressed genes between wild-type and *Med12*-mutant cells
1164 separately in pluripotency conditions, the Epi- and PrE-cluster.
1165
1166 **Supp Table 7**: Oligos used as gRNAs or PCR primers.
1167

1168 # Supplementary Movie legends

1169 **Supp Movie 1**: Timelapse imaging of H2B-Cerulean (blue) and iGata6-mCherry expression
1170 (red) in wild-type and Med12-mutant cells during Epi and PrE differentiation under same
1171 conditions as in Figure 3E. Following time lapse imaging, cells were immunostained for the
1172 Epi-marker NANOG (green) and the PrE marker SOX17 (magenta). Nuclei in immunostainings
1173 labelled with Hoechst dye (cyan). Scale bar: 50 µm.